Unique metabolic profiles of *Blautia wexlerae* achieve beneficial effects for the control of obesity and type 2 diabetes

Koji Hosomi
National Institutes of Biomedical Innovation, Health and Nutrition
Mayu Saito
Noster Inc.
Jonguk Park
National Institutes of Biomedical Innovation, Health and Nutrition
Haruka Murakami
Ritsumeikan University
Naoko Shibata
Waseda University
Masahiro Ando
Waseda University
Takahiro Nagatake
National Institutes of Biomedical Innovation, Health and Nutrition
Kana Konishi
Toyo University
Harumi Ohno
Kiryu University
Kumpei Tanisawa
Waseda University
Attayeb Mohsen
National Institutes of Biomedical Innovation, Health and Nutrition
Yi-An Chen
National Institutes of Biomedical Innovation, Health and Nutrition
Hitoshi Kawashima
National Institutes of Biomedical Innovation, Health and Nutrition
Yayoi Natsume-Kitatani
National Institutes of Biomedical Innovation, Health and Nutrition
Yoshimasa Oka
Noster Inc.
Hidenori Shimizu

Noster Inc.
Mari Furuta
National Institutes of Biomedical Innovation, Health and Nutrition
Yoko Tojima
National Institutes of Biomedical Innovation, Health and Nutrition
Kento Sawane
National Institutes of Biomedical Innovation, Health and Nutrition
Azusa Saika
National Institutes of Biomedical Innovation, Health and Nutrition
Yasunori Yonejima
Noster Inc.
Haruko Takeyama
Waseda University
Akira Matsutani
Shunan City Shinnanyo Hospital
Kenji Mizuguchi
National Institutes of Biomedical Innovation, Health and Nutrition
Motohiko Miyachi
National Institutes of Biomedical Innovation, Health and Nutrition
Jun Kunisawa (✉ kunisawa@nibiohn.go.jp)
National Institutes of Biomedical Innovation, Health and Nutrition

---

Research Article

Keywords: human gut microbiota, bacterial metabolites, anti-inflammation, anti-adipogenesis, mitochondrial metabolism, cross-feeding

Posted Date: January 27th, 2022

DOI: https://doi.org/10.21203/rs.3.rs-1259439/v1

Version of Record: A version of this preprint was published at Nature Communications on August 18th, 2022. See the published version at https://doi.org/10.1038/s41467-022-32015-7.

Abstract

The gut microbiome is an important determinant in various diseases. Here we performed a cross-sectional study of Japanese adults and identified the *Blautia* genus, especially *B. wexlerae*, as a commensal bacterium that is inversely correlated with obesity and type 2 diabetes mellitus. Oral administration of *B. wexlerae* to mice induced metabolic changes and anti-inflammatory effects that decreased both high-fat diet–induced obesity and diabetes. The beneficial effects of *B. wexlerae* were mediated directly by unique amino-acid metabolism to produce S-adenosylmethionine, acetylcholine, and l-ornithine and indirectly by carbohydrate metabolism resulting in the accumulation of amylopectin and production of succinate, lactate, and acetate and simultaneous modification of the gut bacterial composition. These findings reveal unique regulatory pathways of host and microbial metabolism that may provide novel strategies in preventive and therapeutic approaches for metabolic disorders.

Introduction

Because of its rising prevalence and associated comorbidities such as type 2 diabetes mellitus (T2DM), obesity is a major public-health concern [1]. T2DM, which is caused by genetic background, overnutrition, and other environmental factors, is a global epidemic disease that is characterized by inflammation, metabolic disorders such as insulin resistance, and β-cell dysfunction [2].

In mammals, white adipose tissue (WAT), the primary site of energy storage, tightly controls glucose homeostasis [3]. During obesity, WAT becomes dysfunctional and thus fails to expand appropriately to store surplus energy. At the whole-body level, this WAT dysfunction causes ectopic fat deposition in other tissues that regulate metabolic homeostasis, leading to progressive insulin resistance and an increased risk of T2DM [3]. In dysfunctional WAT, adipocyte hypertrophy is accompanied by a shift to an adverse adipokine secretory profile, which typically includes elevated pro-inflammatory factors such as TNF-α. As obesity progresses, chemotactic signals including MCP1 and S100a8 recruit monocytes and macrophages, respectively, which infiltrate obese WAT to fuel an inflammatory milieu [4,5]. Macrophages dysregulate local adipocyte signaling and impair whole-body insulin sensitivity by creating ‘crown-like’ structures [3,5].

The gut microbiota is recognized as a key environmental factor that contributes to the pathophysiology of obesity [6–8] and T2DM [9–11]. In several studies using human and animal models, gut microbial transplantation led to the transfer of obesity and T2DM phenotypes [12–14]. The gut microbiota produces a wide range of metabolites, some of which appear to be causative disease factors. For example, because increased intestinal permeability is a characteristic of human T2DM, gut bacterial lipopolysaccharide can induces a metabolic endotoxemia that is a triggering factor for the onset of insulin resistance [15]. The gut microbiota largely promotes energy storage by decreasing thermogenesis in induced brown adipose tissue and promoting WAT expansion [16]. Tryptophan-derived metabolites from the gut microbiota control

microRNA expression in WAT to regulate metabolism and inflammation, leading to obesity and insulin resistance [17].

In contrast to the gut microbiota's disease-promoting effects, the short-chain fatty acids (SCFAs) and secondary bile acids generated by microbes are known to have anti-obesity and anti-diabetes properties. For example, butyrate suppresses inflammation through the inhibition of NF-κB activity and induction of regulatory T cells [18,19]. In addition, butyrate acts as a ligand for G-protein–coupled receptors (GPCR41 and GPCR43) in the gut and promotes the release of gut hormones, including GLP-1, PYY, and GLP-2 [12]. Together with butyrate, the SCFAs propionate and acetate increase fatty acid oxidation and reducing of fatty acid synthesis in PPARγ dependent manner to ameliorate obesity and consequently T2DM [12,20]. Furthermore, secondary bile acids generated by the gut microbiota activate the membrane bile acid receptor to induce the production of GLP-1 [12].

Consistent with the pivotal role of the gut microbiota in the control of adipose tissue, obese persons and patients with T2DM have an altered gut microbial composition [13]. For example, diabetic European women demonstrate alterations in the composition and function of the gut microbiota [10]. Of note, the mathematical model established from their metagenomic profiles identified T2DM with high accuracy among Europeans—but not Chinese people—indicating that the discriminant metagenomic markers for T2DM differ between European and Chinese populations [10]. Several lines of evidence have indicated regional differences in gut microbial composition [21,22], which are influenced by various environmental factors including diet [23–25] and genetic background [8,26]. However, the mechanisms underlying the effects of differences in gut microbial composition on obesity and T2DM remain poorly understood.

Japanese people have a unique dietary culture and habits, and their gut microbiome shows greater abundance in the genera *Bifidobacterium* and *Blautia* compared with those of people in other countries [22]. Several studies have investigated the gut microbiota of Japanese subjects and its association with obesity and T2DM. For example, one group [27] used 16S rRNA amplicon sequencing to analyze 10 subjects (4 non-obese and 6 obese), and others [28,29] applied a reverse transcription-quantitative PCR method to evaluate Japanese patients with T2DM (50 or 19 subjects). In addition to their unique gut microbial composition, Japanese people exhibit the highest average life span worldwide and a very low body mass index (BMI) [30]; therefore a study involving Japanese participants may increase our understanding of the gut microbiota and its contributions to ameliorating obesity and T2DM.

Here we conducted a cross-sectional study of Japanese adults and found that the abundance of *Blautia wexlerae* was inversely correlated with obesity and T2DM. In addition, the administration of *B. wexlerae* causatively decreased high-fat diet–induced obesity and diabetes in mice. Furthermore, we identified several unique metabolites of *B. wexlerae* that altered energy metabolism, exerted anti-inflammatory effects, and changed the composition of the gut bacterial environment.

Results

Japanese cohort study

We conducted a cross-sectional study of 217 participants to assess the association between the gut microbiota and obesity or T2DM in Japanese adults (Table S1). Multiple-regression analysis revealed high correlation between the gut microbiota and BMI (R^2 = 0.32) and T2DM (R^2 = 0.29). Multiple regression analysis to explore gut microbiome alterations in obesity identified 16 genera that were related to BMI (Table S2), among which 11 organisms were selected according to the R-squared score from single regression analysis (Fig. 1A). In the same way, combining multiple logistic regression analysis and single logistic regression analysis found 8 organisms that were differentially abundant in samples from T2DM patients compared with control subjects (Fig. 1B, Table S3). Obesity (BMI ≥ 25) and T2DM were commonly associated with decreased abundance of *Blautia*, *Faecalibacterium*, and *Butyricicoccus* and an increase in *Megasphaera* abundance (Fig. 1C, S1A, S1B). *Faecalibacterium* and *Butyricicoccus* are known butyrate-producing bacteria [13,31], and previous studies showed potential beneficial roles of *Faecalibacterium* in both human cohorts and animal models [13].

Although several studies have implicated the involvement of *Blautia* in the development of obesity and T2DM [13,32], little definitive information is available. We therefore assessed the effect of *Blautia* on obesity and T2DM via evaluating the odds ratio (OR) and learned that the *Blautia* abundance was inversely correlated to the ORs of obesity and T2DM (Fig. 1D, Table S4, S5). Notably, because *Blautia* was highly discriminant for obesity and T2DM in our Japanese population, we subsequently focused this study on the role of *Blautia* in the control of obesity and diabetes.

We next investigated whether factors other than the prevalent obesity and T2DM, such as age, sex, and medication (e.g., metformin), influenced the proportion of *Blautia* [33] but found no association between *Blautia* abundance and these factors (Fig. S2). Furthermore, we tested the gut microbiome composition in nonDM and T2DM samples by using data sets randomly selected from study participants that were similarly distributed in terms of age and sex. *Blautia* abundance was significantly increased in the adjusted nonDM samples compared with T2DM samples (Table S6), suggesting little confounding effect of these factors such as age and sex on this analysis.

We then used the sequences of representative operational taxonomic units (OTUs) as query strings in BLASTN searches to estimate which species of the *Blautia* genus were inversely associated with obesity and T2DM; this analysis returned three *Blautia* species—*B. wexlerae*, *B. glucerasea*, and *B. stercoris*. Among these, *B. wexlerae*, especially OTU GQ448486.1.1387, predominated, and the relative abundance of OTU GQ448486.1.1387 was nearly equal to that of *Blautia* overall (Fig. 1E, S3). Together, these findings suggest *B. wexlerae* as a candidate gut microbe that might potently ameliorate obesity and T2DM.

Oral administration of B. wexlerae modulated the phenotypes of high-fat diet–induced obesity and diabetes in mice

Given the findings from our human cohort study, we turned to a murine model to examine the causality of *B. wexlerae* in obesity and diabetes. Compared with lean mice fed a standard chow diet (CD-fed mice), obese mice fed a high-fat diet (HFD-fed mice) had increased body weight, accumulation of peritesticular fat, and increased epididymal adipose tissue (eAT) weight (Fig. 2A–2C). Oral supplementation with *B. wexlerae* had no effect on mice's food consumption (Fig. S4). However, oral administration of *B. wexlerae* during HFD feeding protected mice from becoming obese, concurrent with decreased body weight gain and fat accumulation, compared with nonsupplemented HFD-fed mice. These results indicate that *B. wexlerae* plays a causative role in the prevention of obesity (Fig. 2A–2C).

We next examined the pathology associated with the obesity-induced diabetes. Compared with CD-fed mice, HFD-fed mice showed increased blood levels of glucose and insulin under fasting conditions and increased plasma HOMA-IR, an indicator of insulin resistance (Fig. 2D–2F); administration of *B. wexlerae* decreased these diabetes indicators in HFD-fed mice (Fig. 2D–2F). During intraperitoneal glucose tolerance testing (IPGTT), CD-fed mice showed the expected transient increases in blood insulin, followed by rapid return to the original level, after intraperitoneal injection of glucose (Fig. 2G). In comparison, glucose injection had no effect on blood insulin levels in HFD-fed mice (Fig. 2G), but HFD-fed mice supplemented with *B. wexlerae* showed similar responses in blood insulin to those of CD-fed mice (Fig. 2G). Consistent with these results, the increases in blood glucose after intraperitoneal glucose injection in HFD-fed mice were normalized to the levels of CD-fed mice when HFD-fed mice were given *B. wexlerae* (Fig. 2H).

Inflammation in the eAT contributes to the development of obesity-induced diabetes. We therefore histologically analyzed the eAT in HFD-fed mice and found macrophages that were accumulated into 'crown-like structures', which are a histological hallmark of inflammation (Fig. 2I, 2J). Consistent with the inhibitory effects of *B. wexlerae* on diabetes pathogenesis, the eAT of HFD-fed mice that received *B. wexlerae* showed little macrophage accumulation (Fig. 2I, 2J). Along the same lines, RT-qPCR analysis indicated that the expression of *Tnfa*, which encodes an inflammatory cytokine, and *S100a8*, which codes for a chemokine that recruits macrophages, were decreased in the mature adipocyte fraction (MAF) in the eAT of HFD-fed mice given *B. wexlerae* (Fig. 2K). Therefore, the administration of *B. wexlerae* inhibited not only body weight gain but also inflammatory responses in the eAT of HFD-fed mice, thus explaining—at least in part—the organism's inhibitory effects on diabetes.

Metabolites from B. wexlerae had direct effects on adipocytes to inhibit inflammation and adipogenesis

The decreased expression of proinflammatory cytokines in adipocytes from mice prompted us to use *in vitro* differentiated adipocytes to examine whether *B. wexlerae* directly affected their proinflammatory cytokine production. During the differentiation of 3T3L1 pre-adipocytes into adipocytes *in vitro*, we treated the cells with the supernatants from *B. wexlerae* cultures (Fig. S5A). Upon differentiation, *B. wexlerae*-untreated 3T3L1 cells expressed increased levels of *Pparγ*, a transcription factor used as a marker of adipocyte differentiation; treatment with *B. wexlerae*-cultured medium did not alter *Pparγ* expression levels (Fig. 3A), suggesting that molecules produced by *B. wexlerae* and present in the culture

supernatant did not affect adipocyte differentiation. Under these same experimental conditions, treatment of 3T3L1 adipocytes with *B. wexlerae*-cultured supernatant reduced the expression of *S100a8* with little effect on *Tnfa* expression (Fig. 3A, S5B), thus indicating that *B. wexlerae*-derived metabolites directly inhibited S100a8 expression in adipocytes.

Several studies have suggested an association between impaired mitochondrial function and diabetes pathogenesis or inflammation [34,35]. We therefore assessed the gene expression of nuclear respiratory factor 1 (Nrf1), a transcriptional factor used as a marker of mitochondrial biogenesis [36]; the addition of *B. wexlerae*-cultured medium increased *Nrf1* expression in 3T3L1 adipocytes (Fig. 3A). Consistent with these gene expression data, flow cytometry using Mitogreen detected increased mitochondrial mass in 3T3L1 adipocytes treated with *B. wexlerae* culture supernatant (Fig. 3B). Functionally, treating 3T3L1 adipocytes with *B. wexlerae*-cultured medium increased mitochondrial basal respiratory oxygen consumption, characterized by increased proton leakage and decreased ATP synthesis, but did not affect glycolysis (Fig. 3C, S6A, S6B), thus suggesting mitochondrial uncoupling for promoting energy expenditure. We also investigated lipid metabolism and found that, upon differentiation, 3T3L1 cells formed lipid drops in the cytoplasm, which were detected by oil red O staining. Consistent with the results of our *in vivo* experiments (Fig. 2C), the treatment of 3T3L1 adipocytes with *B. wexlerae*-cultured medium decreased lipid accumulation in a dose-dependent manner (Fig. 3D).

We then aimed to confirm these phenomena *in vivo*. Indeed, the expression of *Nrf1* was reduced in the eAT mature adipocyte fraction (MAF) of HFD-fed mice compared with CD-fed mice, and the administration of *B. wexlerae* to HFD-fed mice increased *Nrf1* expression (Fig. 3E), suggesting altered mitochondrial metabolism in the obese mice. Therefore, we next examined energy metabolism through liquid chromatography–tandem mass spectrometry (LC-MS/MS) of eAT MAF. Signals associated with representative metabolites of glycolysis (lactate) and the TCA cycle (citrate, isocitrate, and succinate) were decreased in HFD-fed mice compared with CD-fed mice (Fig. 3F), indicating metabolic abnormalities associated with obesity and diabetes, similar to results from a previous study [37]. The administration of *B. wexlerae* to HFD-fed mice did not affect their lactate level but increased their isocitrate and succinate levels (Fig. 3F), suggesting that *B. wexlerae* stimulates mitochondrial metabolism. This result was supported by the presence of increased acetyl-l-carnitine, a constituent of the inner mitochondrial membrane [38,39], in the eAT MAF of HFD-fed mice that received *B. wexlerae* (Fig. 3G). These findings collectively indicate that *B. wexlerae* produces metabolites that modify host inflammatory responses and mitochondria-associated energy metabolism.

Metabolic pathways of B. wexlerae and their unique metabolites

To identify *B. wexlerae*-derived metabolites beneficial for controlling obesity and diabetes, we first sought to reveal the metabolic uniqueness of *Blautia* on the basis of genetic information. Using iPATH3.0 [40], we compared the presence of Kyoto Encyclopedia of Genes and Genomes (KEGG) orthologous groups [41] among *Blautia* (KEGG organism code: rob), *Bacteroides* (KEGG organism code: bvu), *Prevotella* (KEGG organism code: pru), and *Faecalibacterium* (KEGG organism code: fpr), which are major intestinal genera

in healthy Japanese individuals [42] (Fig. S7A). This analysis revealed 61 KEGG orthologous groups that were unique to *Blautia*, and TargetMine identified 10 enriched pathways ($P < 0.01$, Benjamini–Hochberg correction) in the metabolic pathway map. Together these results suggest various unique features of *Blautia* in regard to amino acid, carbohydrate, and nucleotide metabolism (Fig. 4A, S7B).

These findings prompted us to analyze the supernatant from *B. wexlerae* cultures by using LC-MS/MS. Data analysis of the resulting volcano plot revealed 7 metabolites that were increased more than 4-fold in the supernatant of *B. wexlerae* cultures compared with uncultured, fresh medium (Fig. 4B). Furthermore, among these 7 metabolites, high levels of S-adenosylmethionine, acetylcholine, and l-ornithine were specifically detected in *B. wexlerae*-cultured supernatant compared with those from cultures of other major intestinal bacteria (i.e., *Bacteroides vulgatus*, *Prevotella copri*, *Faecalibacterium prausnitzii*) (Fig. 4C).

In the S-adenosylmethionine cycle, *B. wexlerae* appears to convert extracellular S-adenosylhomocysteine to S-adenosylmethionine via intermediates such as homocysteine and methionine (Fig. S8A). Although other intestinal bacteria likewise uptake S-adenosylhomocysteine into the cell, its subsequent metabolism appears to be different (Fig. S8A). The pathway in *F. prausnitzii* is unclear, but *B. vulgatus* and *P. copri* produce homocysteine and cysteine from S-adenosylhomocysteine rather than S-adenosylmethionine (Fig. S8A).

Acetylcholine typically is biosynthesized from serine via ethanolamine and choline [43]. Indeed, serine—but not choline—was decreased in *B. wexlerae*-cultured supernatant but not in that from other major intestinal bacteria, suggesting that *B. wexlerae* may uniquely utilize extracellular serine rather than choline to synthesize acetylcholine (Fig. S8B). Furthermore, citrulline, arginine, and ornithine are central metabolites of the urea cycle [44]. However, citrulline and arginine contents were decreased in the supernatant from cultures of *B. wexlerae* compared with other major intestinal bacteria, suggesting that *B. wexlerae* exclusively utilizes extracellular citrulline and arginine to produce ornithine (Fig. S8C). Therefore, *B. wexlerae* has several unique metabolic characteristics regarding amino acid synthesis and consequently produces unique metabolites.

S-adenosylmethionine, acetylcholine, and ornithine have anti-inflammatory properties and modify aspects of host metabolism, such as lipid metabolism, indicating that these compounds are potential effector metabolites for controlling obesity and diabetes. To address this hypothesis, we examined the effects of these metabolites on 3T3L1 adipocytes. Treatment of these cells with S-adenosylmethionine, acetylcholine, or ornithine decreased lipid accumulation in a dose-dependent manner (Fig. 4D); S-adenosylmethionine also suppressed the expression of *S100a8* (Fig. 4E).

Administration of B. wexlerae to mice modified their intestinal environment

To identify additional *B. wexlerae* candidate molecules for the control of obesity and diabetes other than those associated with amino acid metabolism, we performed comprehensive Raman spectroscopic analysis to detect multiple molecules simultaneously without labeling [45,46]. As a control signal, the

Raman spectra for total protein were identical among *B. wexlerae*, *B. vulgatus*, *P. copri*, and *F. prausnitzii* (Fig. 5A). In contrast, the spectrum characteristic of *B. wexlerae* was extracted by MCR multivariate analysis. This spectrum has a sharp peak at 480 cm^{-1} and several Raman bands attributed to carbohydrates are observed in the 800-1500 cm^{-1} region. These all bands are assigned to amylose and amylopectin [47]. The corresponding intensity images indicate that these polysaccharides are highly accumulated in *B. wexlerae* and *F. prausnitzii* cells, but only slightly in *B. vulgatus* and *P. copri* cells (Fig. 5A). Plotting the intracellular mean intensity also shows the same tendency with variation among single cells, suggesting that some *B. wexlerae* cells have a large amount of accumulation.

Starch consists of amylose and amylopectin, which are linear and branched, respectively, polymers of glucose units. The amylose content was similar among *B. wexlerae*, *B. vulgatus*, *P. copri*, and *F. prausnitzii* (Fig. 5B). In contrast, amylopectin was more abundant in *B. wexlerae* than in *B. vulgatus* and *P. copri* but similar to that in *F. prausnitzii*, the carbohydrate preferences of which have been predicted through *in silico* techniques [48] (Fig. 5B). Consistent with these findings, genomic information (GenBank accession no. CZAW01000000) indicates that *B. wexlerae* harbors the necessary metabolic enzymes for the *de novo* synthesis of starch from glucose and sucrose (Fig. S9). Therefore, the high concentration of starch observed in *B. wexlerae* was likely due to its high amylopectin content.

Bacterial metabolization of amylose and amylopectin results in the generation of several SCFAs [49], and genomic information (GenBank accession no. CZAW01000000) indicates that *B. wexlerae* conserves various enzymes necessary for the production of succinate, lactate, and acetate but lacks production pathways for propionate and butyrate (Fig. S10). Indeed, succinate, lactate, and acetate contents were increased in *B. wexlerae*-cultured medium compared with fresh medium, but propionate and butyrate levels were similar between cultured and fresh media (Fig. 5C). In addition, the concentration of succinate in the supernatant from *B. wexlerae* cultures was higher than that from *P. copri* and *F. prausnitzii* and similar to that from *B. vulgatus* (Fig. 5C, S11). Furthermore, lactate and acetate were more abundant in the supernatants from cultures of *B. wexlerae* than from other bacteria (Fig. 5C, S11). Together, these findings indicate that *B. wexlerae* utilizes abundantly stored starch (i.e., amylopectin) and produces increased levels of succinate, lactate, and acetate.

Because cross-feeding, such as the utilization of acetate by butyrate-producing bacteria, is an important metabolic interaction among intestinal bacteria [49,50], we next examined the concentrations of various SCFAs in fecal samples from mice. In the results, propionate and butyrate were somewhat decreased and acetate was markedly reduced in feces from HFD-fed mice compared with CD-fed mice (Fig. 5D). In contrast, the administration of *B. wexlerae* to HFD-fed mice increased fecal levels of acetate, propionate, and butyrate (Fig. 5D). None of the groups of mice yielded detectable fecal levels of succinate or lactate (data not shown). These findings collectively suggest that *B. wexlerae* does not produce propionate and butyrate but supplies substrates such as succinate, lactate, and acetate to other gut commensal bacteria, consequently leading to the increased levels of propionate and butyrate in feces.

Furthermore, to consider the influence of *B. wexlerae* on the composition of other commensal bacteria in the gut, we used 16S rRNA sequencing analysis to examine fecal bacterial composition in mice. Consistent with previous reports [49], principal coordinate analysis (PCoA) revealed that gut bacterial composition differed between HFD- and CD-fed mice (Fig. 5E). When HFD-fed mice were treated with *B. wexlerae*, their bacterial composition was closer to (but still different from) that of HFD-fed mice than CD-fed mice (Fig. 5E).

Linear discriminant analysis effect size [51] provided a ranked list of intestinal bacteria that differed between nonsupplemented HFD-fed mice and HFD-fed mice given *B. wexlerae* (Fig. 5F). At the genus level, *Lachnospiraceae NK4A136 group* was increased in HFD-fed mice compared with HFD-fed mice given *B. wexlerae*, which were similar to CD-fed mice in regard to these organisms (Fig. S12). In contrast, the proportions of *Rikenellaceae RC9 gut group* and *Alistipes* were decreased in HFD-fed mice compared with CD-fed mice; the administration of *B. wexlerae* to HFD-fed mice increased these organisms to similar levels as in CD-fed mice (Fig. S12). Furthermore, the proportion of *Akkermansia* was increased in HFD-fed mice compared with CD-fed mice and increased further upon administration of *B. wexlerae* (Fig. S12). Therefore, the administration of *B. wexlerae* likely changed the gut bacterial composition to increase the SCFA production capacity by increasing *Rikenellaceae RC9 gut group*, *Alistipes*, and *Akkermansia*, all of which produce propionate, butyrate, or both [52–54].

These results from our mouse experiments provided feedback for our human data analysis. Among the 15 bacterial genera that were related to obesity and T2DM in our Japanese cohort (Fig. 1), the *Blautia* genus was positively correlated with several genera, especially *Butyricicoccu*s, which is a butyrate-producing bacterium [54] (Fig. 6A, 6B). This relationship suggests that *Blautia* might influence features of the intestinal environment, such as SCFA production, in collaboration with other intestinal bacteria. To address this hypothesis, we examined the effects of *B. wexlerae*-derived metabolites on the growth and SCFA production of *Butyricicoccus faecihominis*, a dominant species of the *Butyricicoccus* genus (Fig. 6C).

Butyricicoccus faecihominis was grown anaerobically and monitored at OD_{595}. The absorbance of *B. faecihominis* at 48 h was increased dose-dependently according to supplementation with *B. wexlerae*-cultured supernatant (Fig. 6D). Consistent with this finding, supplementation with acetate, a product of *B. wexlerae*, likewise increased the growth of *B. faecihominis* (Fig. 6E). In addition, supplementation with *B. wexlerae*-cultured supernatant or acetate increased the amount of butyrate produced by *B. faecihominis* (Fig. 6F). These findings indicate a metabolic interaction between *B. wexlerae* and *B. faecihominis*, a butyrate-producing intestinal bacterium; this interaction may, in turn, improve various aspects of the intestinal environment, such as butyrate production.

Discussion

By combining human cohort data and animal experiments, we have demonstrated that *Blautia wexlerae* has potent effects for reducing obesity and T2DM. Our human cohort study showed that intestinal *B.*

wexlerae reduces the risk of obesity and diabetes in Japanese adults. As an underlying mechanism, *B. wexlerae* contains several amino acid metabolites (i.e., S-adenosylmethionine, acetylcholine, l-ornithine) that confer anti-adipogenesis and anti-inflammatory properties to adipocytes. In addition, *B. wexlerae* contains a high amount of starch (i.e., amylopectin) and produces carbohydrate metabolites (i.e., succinate, lactate, acetate) to consequently modify the gut environment, including the bacterial and SCFA composition of the gut microbiota. Thus, *B. wexlerae* offers various, numerous, and diverse benefits for health maintenance.

Accumulating evidence reveals several human intestinal bacteria associated with obesity and T2DM. For example, the genera of *Bifidobacterium*, *Faecalibacterium*, *Roseburia*, and *Akkermansia* are inversely associated with obesity and T2DM, are beneficial to human health, and may be useful as probiotics [55–57]. Indeed, in our Japanese cohort, *Bifidobacterium* and *Faecalibacterium* emerged as beneficial bacterial genera inversely associated with BMI or T2DM. Although reported less frequently than *Bifidobacterium* and *Faecalibacterium*, the genera *Megasphaera* and *Ruminococcus* are both associated with obesity or T2DM [13,58], consistent with our results.

Several previous human studies have indicated the involvement of intestinal *Blautia* in obesity and T2DM, but whether *Blautia* contributes to aggravation or amelioration of these disorders is unclear [13,59]. For example, in Russian subjects, disorders of glucose metabolism, such as high fasting glucose levels, were associated with increased prevalence of *Blautia* [60]. In contrast, a European study found no significant correlation between *Blautia* and obesity or T2DM [10]. However, a Spanish study of the childhood microbiome and its association with the metabolic complications underlying obesity revealed that *Blautia* species, including *B. wexlerae*, were associated with normal-weight children and negatively correlated with fecal inflammatory cytokines such as TNF-α [61]. In addition, a previous Japanese cohort study reported that *Blautia* was significantly and inversely associated with visceral fat area, regardless of sex [32]. In view of these apparent inconsistencies, it is important to remember that regional variation in human gut microbial composition occurs. Indeed, the genus *Blautia* is more abundant in the gut microbiota of Japanese people than those of other countries [22], and studies involving Japanese cohorts consistently indicate beneficial effects of *Blautia*. Furthermore, at the species level, the *Blautia* genus includes several OTUs; OTU GQ448486.1.1387 of *B. wexlerae* was dominant in our Japanese cohort, but we wonder which species are abundant in other geographic regions. Given that our current study identified multiple health-promoting molecules in *B. wexlerae*, the inconsistent findings among other studies might be clarified by examining the differences among bacterial strains in light of their activity to produce beneficial metabolites.

In this regard, we identified several products of *B. wexlerae* amino acid metabolism that can contribute to the control of obesity and diabetes. Acetylcholine is a neurotransmitter and an agonist for the alpha-7 nicotinic acetylcholine receptor, which is expressed on adipocytes and is a potent therapeutic target for inflammatory diseases, including T2DM and obesity [62–65]. In addition, numerous central neurotransmitters are present in the gastrointestinal tract, where their local effects include modulating gut

motility and cell signaling [66]. The absence of a gut microbiota is associated with significant reduction in the intestinal levels of these neurotransmitters, suggesting that gut microbes are important producers of neurotransmitters [66]. Although *Lactobacillus plantarum*, which was isolated from a fermented food (sauerkraut), is known to synthesize acetylcholine [67], no human intestinal acetylcholine-producing bacteria had been identified previously. We here revealed that the human intestinal bacteria *B. wexlerae* produces acetylcholine. An interesting potential subject for future study is that the acetylcholine synthetic pathway of *B. wexlerae* lacks homologs of mammalian enzymes (data not shown).

Another *B. wexlerae*-derived amino acid metabolite that we identified is l-ornithine; its beneficial effects include roles in detoxifying ammonia, as an intermediate in the urea cycle, and in modulating host lipid metabolism [68,69]. Intriguingly, even though l-ornithine is a nutrient necessary for health maintenance, it is difficult to obtain sufficient l-ornithine from ordinary diets; most foods have only scant levels of l-ornithine [68]. In addition, a lack of intestinal bacteria reportedly hampers hepatic l-ornithine homeostasis in mice [70]. These previous and our current findings together support the importance of intestinal bacteria, including *Blautia*, in the supply of l-ornithine for health maintenance.

S-adenosylmethionine, a third *B. wexlerae*-derived metabolite, acts as a methyl donor for biologic methylation and helps to prevent diabetes, obesity, and inflammation [71,72]. In addition, S-adenosylmethionine is applied in the treatment of depression, osteoarthritis, and liver diseases [73]. Because S-adenosylmethionine is therefore an important substance in health maintenance, this metabolite and the microbes that produce it have garnered attention in regard to their applications in the pharmaceutical and food industries [74]. However, the mechanisms through which intestinal bacteria produce and supply S-adenosylmethionine are not well understood [75,76]. Our findings that *B. wexlerae*, an intestinal bacterium, produces S-adenosylmethionine, l-ornithine, and acetylcholine collectively point to the importance of amino acid metabolism by gut microbiota both in the development of metabolic disorders such as obesity and T2DM and in strategies for their prevention and treatment.

Starch is one of the main forms of carbohydrate in the diet [77]. Digestible starches are broken down by enzymes in the small intestine and then absorbed. In contrast, indigestible resistant starches pass into the colon, where they induce physiologic consequences including improvements in glucose tolerance and insulin response via modification of gut environment such as SCFA condition [77]. The indigestible components of plant foods, such as cell wall materials, are rich sources of dietary fiber. In the current study, we revealed that *B. wexlerae* contains high concentrations of starch, especially amylopectin. We think that when a probiotic containing *B. wexlerae* is administered, the starch concentrated in *B. wexlerae* acts as ‘bacterial fiber’ that affects the gut environment, much like the dietary fiber provided from plants. Indeed, oral supplementation with *B. wexlerae* influenced gut microbial composition and increased fecal propionate and butyrate levels in mice, even though *B. wexlerae* itself cannot produce these SCFAs. In addition to providing starch, *B. wexlerae* generates succinate, lactate, and acetate through carbohydrate metabolism. Acetate is utilized by butyrate-producing bacteria to produce butyrate [49,50,78]. Indeed, our current study revealed the cooperative effects of *B. wexlerae* on butyrate production by *Butyricicoccus*.

Intestinal bacteria also utilize succinate and lactate, converting them into propionate or butyrate [79]. In this regard, *B. faecihominis* appeared to produce propionate in addition to butyrate, albeit at lower levels, and supplementation with succinate enhanced the organism's propionate production. In terms of bacterial cross-feeding, *Bifidobacterium* is a well-known provider of acetate and lactate—but not succinate [79,80]. *Blautia wexlerae*, which generates succinate in addition to acetate and lactate, seems to be a key microbial player in driving metabolic conditions in the gut. Overall, carbohydrate metabolism in *B. wexlerae* appears to improve the gut environment, leading to amelioration of metabolic disorders.

In summary, we identified *B. wexlerae* as a potent beneficial human intestinal bacterium with anti-inflammatory properties and the ability to modify the host gut environment and lipid metabolism. Regarding the mechanisms underlying these benefits, we elucidated characteristics of *B. wexlerae*'s amino acid and carbohydrate pathways, in which multiple metabolites appear to act cooperatively to ameliorate metabolic disorders including obesity and diabetes. The discovery of a novel metabolic role of the gut microbiota in the pathophysiology of obesity and T2DM reveals opportunities for the development of new preventive methods (e.g., probiotics) and therapeutic approaches for metabolic disorders.

Materials And Methods

Collection of human samples

Diabetic patients were recruited at Shinnanyo Hospital, Shunan City, Yamaguchi, Japan (Table S1); nondiabetic adult volunteers (control subjects) were recruited from surrounding communities (Table S1). From the 242 total possible participants, we excluded 25 who had received antibiotics within the previous 2 weeks (18 subjects), had traveled overseas within the previous month (2 subjects), or had gastrointestinal disease (5 subjects), thus leaving a study population of 217 participants containing 147 nondiabetic subjects, 45 type 2 and 25 type 1 diabetic patients. Fecal samples were collected by using guanidine thiocyanate solution (TechnoSuruga Laboratory Co., Ltd., Shizuoka, Japan) as previously described [81]. Physical measurements, including body weight, height, blood glucose, and HbA1c, and disease information were obtained through medical examinations and from medical records. All experiments were approved by the Ethics Committee of the National Institutes of Biomedical Innovation, Health, and Nutrition and were conducted in accordance with their guidelines (approval number: 177-08). Informed consent was obtained from all participants.

16S rRNA gene amplicon sequencing analysis

DNA was extracted from human fecal samples in guanidine thiocyanate solution by using the bead beating method and an automatic nucleic acid extraction system (Gene Prep Star PI-80X, Kurabo Industries, Ltd., Osaka, Japan) as previously described [81]. DNA was extracted from mouse fecal samples through a slight modification of this method. Briefly, a mouse fecal sample was placed in a 2-ml vial (Wakenbtech Co., Ltd., Tokyo, Japan) containing 0.5 ml of lysis buffer (No. 10, Kurabo Industries, Ltd.) and 0.5 g of 0.1-mm glass beads. The mixture was mechanically disrupted by bead beating by using a

Cell Destroyer PS1000 (Bio Medical Science, Tokyo, Japan) at 4260 rpm for 50 s at room temperature. After centrifugation at 13,000 × *g* for 5 min at room temperature, DNA was extracted from 0.2 ml of the supernatant by using a Gene Prep Star PI-80X device (Kurabo Industries, Ltd.).

The 16S rRNA gene amplicon in human and mouse fecal DNA was sequenced as previously described [81]. The V3–V4 region of the 16S rRNA gene was amplified from the fecal DNA samples by using the following primers: forward, 5'- TCGTCGGCAGCGTCAGATGTGTATAAGCGACAGCCTACGGGNGGCWGCAG-3'; and reverse, 5'-GTCTCGTGGGCTCGGAGATGTGTATAAGAGACAGGACTACHVGGGTATCTAATCC-3' [82]. A DNA library was prepared by using a Nextera kit Set A (Illumina, San Diego, California, USA), and 16S rRNA gene sequencing was performed by using MiSeq (Illumina) in accordance with the manufacturer's instructions. The sequencing results were analyzed using the Quantitative Insights Into Microbial Ecology (QIIME) software package [83] and QIIME Analysis Automating Script (Auto-q) (doi: 10.5281/zenodo.1439555) as previously described [84]. Open-reference operational taxonomic unit (OTU) picking and taxonomy classification were performed based on sequence similarity (>97%) by using UCLUST software [85] with the SILVA v128 reference sequence [86].

Bacterial strains and culture

Blautia wexlerae (JCM 17041), *Bacteroides vulgatus* (JCM 5826), *Prevotella copri* (JCM 13464), *Faecalibacterium prausnitzii* (JCM 31915), and *Butyricicoccus faecihominis* (JCM 31056) were provided by the RIKEN BRC through the National BioResource Project of the MEXT/AMED, Japan. All bacterial strains were cultured anaerobically at 37°C by using an anaerobic chamber (Bactron 300, Toei Kaisha, Ltd., Tokyo, Japan). For oral administration into mice, *B. wexlerae* was cultured anaerobically in reinforced clostridial medium (BD Difco, Franklin Lakes, New Jersey, USA) at 37°C for 48 h until OD_{600} = 1.0–1.5. Cultures were stored as 0.5-ml aliquots at –80°C until use for oral administration into mice. For measurement of starch, SCFAs, and metabolites and Raman spectroscopic analysis, *B. wexlerae*, *B. vulgatus*, *P. copri*, and *F. prausnitzii* were cultured in clostridial reinforced medium (BD Difco) at 37°C for 48 h; at inoculation, OD_{600} was approximately 0.05 for all strains (*B. wexlerae*, 1.0; *B. vulgatus*, 1.1; *P. copri*, 0.8; and *F. prausnitzii*, 0.9). For the cross-feeding assay, *B. faecihominis* was cultured anaerobically at 37°C in GAM broth (Nissui Pharmaceutical Co., Ltd., Tokyo, Japan) supplemented without or with the *B. wexlerae* culture supernatant, succinate acid, sodium lactate, or sodium acetate; the pH of the medium was adjusted to 7.0.

Mice and high-fat diet–induced obesity and diabetes

Male C57BL/6 mice (age, 4 weeks) were purchased from Japan SLC (Shizuoka, Japan). The mice were maintained in the specific pathogen-free animal facility and were fed a standard diet for 2 weeks, followed by a high-fat diet composed of chemically defined materials (Oriental Yeast, Tokyo, Japan) for 2 to 3 months. During the terms, mice received 0.5 ml of bacterial solution by oral gavage 3 times each week. All experiments involving mice were approved by the Animal Care and Use Committee of the

National Institutes of Biomedical Innovation, Health, and Nutrition (approval no. DS27-48R10) and were conducted in accordance with their guidelines.

Intraperitoneal glucose tolerance testing (IPGTT)

IPGTT was performed as described previously [87] with modification. Briefly, mice were fasted overnight (16 h) and then intraperitoneally injected with d-(+)-glucose (2 g/kg body weight; 20% solution, Nacalai Tesque, Kyoto, Japan). To measure the blood glucose level, blood was obtained from the tail vein by cutting with a single-edged blade (Feather, Osaka, Japan) and analyzed on a ONE TOUCH Ultra Vue (LifeScan Japan, Tokyo, Japan) before and after glucose injection at the indicated time points. Blood insulin levels were measured by using an LBIS Mouse Insulin ELISA kit (Wako Pure Chemicals, Osaka, Japan) in accordance with the manufacturer's instructions.

Histological analysis

Frozen tissue was analyzed histologically as described previously with minor modification [88]. Briefly, tissue samples were washed with PBS (Nacalai Tesque) on ice and frozen in Tissue-TeK OCT compound (Sakura Finetek, Tokyo, Japan) in liquid nitrogen. Frozen tissue sections (thickness, 6 μm) were prepared by using a cryostat (model CM3050 S, Leica, Wetzlar, Germany) and were fixed for 30 min at 4°C in prechilled 95% ethanol (Nacalai Tesque) followed by 1 min at room temperature in prechilled 100% acetone (Nacalai Tesque).

For hematoxylin and eosin staining, tissue sections were washed with running water for 10 min, stained with Mayer's hematoxylin solution (Wako Pure Chemicals) for 10 min, and washed with running water for 30 min. Tissue sections were then stained with 1% eosin Y solution (Wako Pure Chemicals) for 1 min, washed with running water for 10 s, and dehydrated through increasing concentrations of ethanol (1 min at each concentration, 70% to 100%, Nacalai Tesque). Tissue sections underwent final dehydration in xylene (Nacalai Tesque) for 3 min and were mounted in Permount (Falma, Tokyo, Japan).

For immunohistological analysis, tissue sections were washed with PBS for 10 min and then blocked in 2% (vol/vol) newborn calf serum in PBS for 30 min at room temperature in an incubation chamber (Cosmo Bio, Tokyo, Japan). Tissue sections were incubated with purified anti-F4/80 monoclonal antibody (1:100; catalog no. 123102, Biolegend, San Diego, California, USA) and BODIPY493/503 (1:1000; catalog no. D3922, Molecular Probes, Eugene, Oregon, USA) in 2% (vol/vol) newborn calf serum in PBS for 16 h at 4°C in the incubation chamber, washed once for 5 min each in 0.1% (vol/vol) Tween-20 (Nacalai Tesque) in PBS and in PBS only, and then stained with Cy3–anti-rat IgG (1:200; catalog no. 712-165-153, Jackson Immuno Research Laboratories, West Grove, Pennsylvania, USA) in 2% (vol/vol) newborn calf serum in PBS for 30 min at room temperature in the incubation chamber. To visualize nuclei, tissue sections then were washed twice (5 min each) with PBS and stained with DAPI (1 μM, AAT Bioquest, Sunnyvale, California, USA) for 10 min at room temperature in the incubation chamber. Finally, tissue sections were washed twice with PBS, mounted in Fluoromount (Diagnostic BioSystems, Pleasanton, California, USA), and examined under a fluorescence microscope (model BZ-9000, Keyence, Osaka, Japan).

Reverse transcription and quantitative PCR (RT-qPCR) analysis

Epididymal adipose tissue (eAT) was minced into Krebs–Ringer bicarbonate HEPES (KRBH) buffer (120 mM NaCl, 4 mM KH_2PO_4, 1 mM $MgSO_4$, 1 mM $CaCl_2$, 10 mM $NaHCO_3$, 30 mM HEPES, 20 μM adenosine, and 4% [wt/vol] BSA) by using scissors, centrifuged to remove blood cells, and then incubated in 2.67 mg/ml collagenase in KRBH buffer for 45 min at 37°C with stirring. The samples were then centrifuged, and the mature adipocyte fraction (MAF, floating fraction) was collected for RT-qPCR testing.

RT-qPCR analysis were performed as described previously [88] with minor modification. Total RNA was isolated from purified or cultured cells by using Sepasol (Nacalai Tesque) and chloroform (Nacalai Tesque), precipitated by using 2-propanol (Nacalai Tesque), and washed with 75% (vol/vol) ethanol (Nacalai Tesque). RNA samples were incubated with DNase I (Invitrogen, Carlsbad, California, USA) to remove contaminating genomic DNA and then reverse-transcribed into cDNA (Superscript III reverse transcriptase, VIRO cDNA Synthesis Kit; Invitrogen).

Quantitative PCR analysis was performed by using a LightCycler 480 II (Roche, Basel, Switzerland) with FastStart Essential DNA Probes Master (Roche) or SYBR Green I Master reagents (Roche). Primer sequences were: *Tnfa* sense, 5'-CTGTAGCCCACGTCGTAGC-3'; *Tnfa* anti-sense, 5'-TTGAGATCCATGCCGTTG-3'; *S100a8* sense, 5'-TCCTTGCGATGGTGATAAAA-3'; *S100a8* anti-sense, 5'-GGCCAGAAGCTCTGCTACTC-3'; *Pparγ* sense, 5'-GAAAGACAACGGACAAATCACC-3'; *Pparγ* anti-sense, 5'-GGGGGTGATATGTTTGAACTTG-3'; *Nrf1* sense, 5'-GCTCTCTGAGACGCTGCTTT-3'; *Nrf1* anti-sense, 5'-GTGTTCAGTTTGGGTCACTCC-3'; *Actinb* sense, 5'-AAGGCCAACCGTGAAAAGAT-3'; and *Actinb* anti-sense, 5'-GTGGTACGACCAGAGGCATAC-3'.

3T3L1 adipocytes

The 3T3L1 cell line (JCRB 9014) was purchased from the Japanese Collection of Research Bioresources (JCRB) cell bank (Osaka, Japan). Differentiation of 3T3L1 adipocytes was performed as previously reported with modifications [89]. 3T3L1 cells were seeded at 3.5×10^4 cells per well in 12-well plates and incubated overnight (16 h) in DMEM (Nacalai Tesque) at 37°C under 5% CO_2 supplemented with 10% (vol/vol) newborn calf serum. The following day, the medium on the cells was changed to DMEM (Nacalai Tesque) supplemented with 10% (vol/vol) fetal bovine serum, and cells were cultured for 3 d; cells were then cultured in adipocyte differentiation medium (0.5 mM isobutyl-methylxanthine [Sigma-Aldrich, St. Louis, Missouri, USA], 1 μM dexamethasone [Sigma-Aldrich], 10 μg/ml insulin [Sigma-Aldrich] in DMEM [Nacalai Tesque] supplemented with 10% [vol/vol] fetal bovine serum) for 2 d and finally in DMEM (Nacalai Tesque) supplemented with 10% (vol/vol) fetal bovine serum for 6 d. During the terms, 1 or 10% *B. wexlerae*-cultured medium or uncultured fresh medium (reinforced clostridial medium [BD Difco]) was added to the 3T3L1 culture medium.

Mitochondrial mass analysis by flow cytometry using Mitogreen

For mitochondrial staining, 3T3L1 adipocytes were incubated with 100 nM Mitogreen (Takara Bio, Shiga, Japan) in PBS supplemented with 2% (vol/vol) newborn calf serum for 15 min at 37°C under 5% CO_2. Stained cells were washed with PBS, treated with trypsin, and then suspended in PBS supplemented with 2% (vol/vol) newborn calf serum. Samples were analyzed by using MACSQuant (Miltenyi Biotec, Bergisch Gladbach, Germany), and data were analyzed by using FlowJo 9.9 (Tree Star, Ashland, Oregon, USA).

Flux analysis

The oxygen consumption rate and extracellular acidification rate were measured by using a flux analyzer (Seahorse Bioscience XF24 Extracellular Flux Analyzer, Agilent, Santa Clara, California, USA) and XF Mito Stress Kit (Agilent). 3T3L1 cells were seed at 3.5×10^3 cells per well in 0.1% gelatin-coated Seahorse 24-well plates and differentiated into adipocytes as described above. After differentiation, *B. wexlerae* culture supernatant or uncultured fresh medium were added to the 3T3L1 adipocyte cultures to a final concentration of 10%; cultures were then incubated at 37°C for 1 h. After incubation, the culture medium was changed to XF Base Medium Minimal DMEM (Agilent) supplemented with 10 mM glucose (Nacalai Tesque), 1 mM pyruvate (Nacalai Tesque), and 2 mM L-glutamine (Nacalai Tesque) for measurement. Compounds injected during the assay and their final concentrations were 1.5 μM oligomycin (inhibitor of ATP synthase), 1 μM FCCP (proton uncoupling agent), and 0.5 μM rotenone + 0.5 μM antimycin A (inhibitors of the mitochondrial respiration complex). XFe Wave software (Agilent) was used to analyze the results.

Oil red O staining

For measurement of lipid accumulation, 3T3L1 adipocytes were washed with PBS for 1 min, treated with 4% paraformaldehyde in PBS (Nacalai Tesque) at 37°C for 30 min, washed with 60% (vol/vol) 2-propanol (Nacalai Tesque), and then dried at 37°C for 15 min. The fixed cells were stained with 0.3% (wt/vol) oil red O (Sigma-Aldrich) in 60% (vol/vol) 2-propanol at 37°C for 30 min, washed with distilled water 3 times, and then incubated with 100% 2-propanol at room temperature for 1 min. Absorbance at 490 nm was measured by using an iMark microplate reader (Bio-Rad, Hercules, California, USA).

LC-MS/MS

Hydrophilic metabolites were extracted as previously described with minor modification [90,91]. The eAT MAF of mice suspended in PBS (Nacalai Tesque) and bacteria-cultured medium (100 μl) were diluted with water (Wako Pure Chemicals) to 200 μl, mixed with 400 μl of methanol (Wako Pure Chemicals) containing methionine sulfone (Wako Pure Chemicals) as an internal standard, and combined with 400 μl of chloroform (Nacalai Tesque). Samples were centrifuged at 20,000 × *g* at 4°C for 15 min, after which 200 μl of supernatant was centrifugally filtered through a 5-kDa cutoff filter (Human Metabolome Technologies, Inc., Tokyo, Japan). The filtrates were lyophilized, resuspended in ultrapure water (Wako Pure Chemicals), and analyzed by LC-MS/MS as previously described [90] by using a Nexera system (Shimadzu, Kyoto, Japan) equipped with two LC-40D pumps, a DGU-405 degasser, an SIL-40C autosampler, a CTO-40C column oven, and a CBM-40 control module, coupled to an LCMS-8050 triple-

quadrupole mass spectrometer (Shimadzu). A pentafluorophenylpropyl column (Discovery HS F5, 150 mm × 2.1 mm, 3 μm; Sigma-Aldrich) was used for the separation of metabolites. Instrument control and data analysis were performed by using the software LabSolutions LCMS with LC/MSMS Method Package for Primary Metabolites, ver. 2 (Shimadzu).

Raman spectroscopic analysis

Raman spectroscopic analysis was performed as described previously with minor modification [92]. Briefly, bacterial cells were cultured anaerobically for 48 h at 37°C, collected by centrifugation at 10,000 × *g* for 10 min at 4°C, and suspended in PBS. The cell suspension was analyzed under a confocal Raman microspectroscopic system, which was equipped with a 100x/1.4N.A. objective lens. The spatial resolution of the system is 0.3×0.3 μm in lateral directions and 2.6 μm in depth direction. The excitation wavelength was 532 nm, and the intensity was 5 mW at the sample point. The mapping scan measurements were performed in steps of 0.25 μm, with the exposure time of 1 second per point.

The data was preprocessed using IGOR Pro software (WaveMetrics, Inc., Lake Oswego, Oregon, USA) for wavenumber calibration and sensitivity correction. Subsequently, a multivariate curve resolution (MCR) analysis was performed on the spectral data set obtained from all the mapping measurements [93]. In the MCR analysis, the decomposed Raman spectra and their corresponding intensity images were calculated by alternating least-squares optimization, based on the initial value spectra created by concatenating the results of the singular value decomposition (SVD) and the reference spectra of glass and PBS.

Measurement of amylose and amylopectin

Bacterial cells were cultured anaerobically for 48 h at 37°C, then collected by centrifugation at 10,000 × *g* for 10 min at 4°C, and frozen at –80°C, and lyophilized (EYELA FDU-2110, Tokyo Rikakikai Co., Ltd., Tokyo, Japan). Amylose and amylopectin contents were measured by using an Amylose/Amylopectin Assay kit (Megazyme, Bray, Ireland) in accordance with the manufacturer's instructions.

SCFA measurement by HPLC

Murine fecal samples were mixed with 95% ethanol (Nacalai Tesque) to a concentration of 100 mg/ml and homogenized by using two 15-s pulses at 6500 rpm from a tissue homogenizer (Precellys 24, Bertin Instruments, Montigny-le-Bretonneux, France) with zirconia beads (Tomy Digital Biology Co., Ltd., Tokyo, Japan). The homogenate was centrifuged at 1600 × *g* for 10 min at 4°C and the supernatant collected. The fecal supernatant or bacterial cultured medium were labeled using an FA Labeling kit (YMC Co., Ltd., Kyoto, Japan) in accordance with the manufacturer's instructions. The labeled samples were analyzed on an HPLC system (Ultimate 3000, Thermo Fisher Scientific, Waltham, Massachusetts, USA) with a 6.0 × 250 mm YMC-Pack FA column (YMC), and the UV spectrum at 400 nm was measured.

Statistical analysis

The output of the QIIME pipeline in Biom table format was imported and analyzed in R (version 3.5.1) (https://www.R-project.org/). The alpha-diversity indices were calculated by using the *estimate_richness* function in the R package 'phyloseq' [94]. The beta-diversity index, calculated according to the Bray–Curtis distance of genus-level data, was generated by using the *vegdist* function in the R package 'vegan' [95]. Principal coordinate analysis (PCoA) was performed by using the *dudi.pco* function in the R package 'ade4' [96], and the PCoA figure was created by using the R package 'ggplot2' [97]. Multiple regression analysis by forward selection and single regression analysis was used to identify the gut microbiota associated with BMI (i.e., *lm* function and step function in the R package 'stats'). Multiple logistic regression analysis by forward selection and single logistic regression analysis were used to identify the gut microbiota associated with obesity and T2DM (i.e., *glm* function and step function in the R package 'stats'). Heatmaps were created by using the R packages 'corrplot' (https://github.com/taiyun/corrplot) and 'superheat' [98]. Statistical significance was evaluated through one-way ANOVA for comparison of multiple groups and the Mann–Whitney *U*-test for two groups by using Prism 7 (GraphPad Software, La Jolla, California, USA) or R package. A *P* value less than 0.05 was considered to be significant.

Data availability

DNA sequencing data have been deposited in the DNA Databank of Japan (DDBJ) under the accession numbers DRA010841 and DRA012134.

Declarations

Acknowledgements

We thank Dr. Tokiko Tabata (Kobe University, Japan) for helpful discussion regarding T2DM and its medication; Mr. Motonobu Sato and Dr. Arihiro Kohara (NIBIOHN) for storing samples; staff in Shunan City and Shunan City Shinnanyo Hospital for sample collection; and members of our laboratories for helpful discussion. This work was supported by the Ministry of Education, Culture, Sports, Science and Technology of Japan (MEXT)/Japan Society for the Promotion of Science KAKENHI (grant numbers 18K17997 and 19K08955 to K.H.; 18H02674, 20H05697, 20K08534, 20K11560, 18H02150, and 17H04134 to J.K.; 16K00944 and 20H04117 to M.M.; 19K07617 to T.N.; and 21K15267 to J.P.); the Japan Agency for Medical Research and Development (AMED; grant numbers JP20ek0410062h0002, 20fk0108145h0001, JP20ak0101068h0004, and JP20gm1010006h004 to J.K.; and 17ek0210078h0002 to H.M.); the Ministry of Health and Welfare of Japan and Public /Private R&D Investment Strategic Expansion PrograM: PRISM (grant number 20AC5004 to J.K.); the Ministry of Health, Labour, and Welfare of Japan (grant numbers JP19KA3001 to K.H.; and 201709002B to MM); Cross-ministerial Strategic Innovation Promotion Program: SIP (grant number 18087292 to J.K.); the Grant for Joint Research Project of the Institute of Medical Science, the University of Tokyo (to J.K.); the Ono Medical Research Foundation (to J.K.); and the Canon Foundation (to J.K.).

Author contributions

K.H. and J.K. designed the study and wrote the manuscript; K.H., H.M., K.K., H.O., K.T., A.Matsutani, and M.M. collected human samples; K.H., J.P., A.Mohsen, Y.A.C., H.K., Y.N.K., and K.M. performed microbiome analysis; K.H., M.S., Y.O., H.S., M.F., Y.T., and Y.Y. performed animal and bacterial experiments; N.S., M.A., and H.T. performed Raman spectroscopic analysis; and K.H., M.F., Y.T., T.N., K.S., and A.S. performed metabolome analysis.

Competing Interest

The authors of this manuscript have the following potential conflicts of interest:

Mayu Saito, Yoshimasa Oka, Hidenori Shimizu, and Yasunori Yonejima are employees of Noster, Inc. (Kyoto, Japan).

References

1. Lobstein, T. *et al.* Child and adolescent obesity: part of a bigger picture. *Lancet* **385**, 2510–2520 (2015).

2. Donath, M. Y. & Shoelson, S. E. Type 2 diabetes as an inflammatory disease. *Nat. Rev. Immunol.* **11**, 98–107 (2011).

3. Kusminski, C. M., Bickel, P. E. & Scherer, P. E. Targeting adipose tissue in the treatment of obesity-associated diabetes. *Nature Reviews Drug Discovery* **15**, 639–660 (2016).

4. Hata, Y. *et al.* Ablation of Myeloid Cell MRP8 Ameliorates Nephrotoxic Serum-induced Glomerulonephritis by Affecting Macrophage Characterization through Intraglomerular Crosstalk. *Sci Rep* **10**, 3056 (2020).

5. Kuwabara, T. *et al.* Macrophage-mediated glucolipotoxicity via myeloid-related protein 8/toll-like receptor 4 signaling in diabetic nephropathy. *Clin. Exp. Nephrol.* **18**, 584–592 (2014).

6. Ley, R. E., Turnbaugh, P. J., Klein, S. & Gordon, J. I. Microbial ecology: human gut microbes associated with obesity. *Nature* **444**, 1022–1023 (2006).

7. Turnbaugh, P. J. *et al.* An obesity-associated gut microbiome with increased capacity for energy harvest. *Nature* **444**, 1027–1031 (2006).

8. Turnbaugh, P. J. *et al.* A core gut microbiome in obese and lean twins. *Nature* **457**, 480–484 (2009).

9. Qin, J. *et al.* A metagenome-wide association study of gut microbiota in type 2 diabetes. *Nature* **490**, 55–60 (2012).

10. Karlsson, F. H. *et al.* Gut metagenome in European women with normal, impaired and diabetic glucose control. *Nature* **498**, 99–103 (2013).

11. Forslund, K. *et al.* Disentangling type 2 diabetes and metformin treatment signatures in the human gut microbiota. *Nature* **528**, 262–266 (2015).

12. Allin, K. H., Nielsen, T. & Pedersen, O. Mechanisms in endocrinology: Gut microbiota in patients with type 2 diabetes mellitus. *Eur. J. Endocrinol.* **172**, R167-177 (2015).

13. Gurung, M. *et al.* Role of gut microbiota in type 2 diabetes pathophysiology. *EBioMedicine* **51**, 102590 (2020).

14. Saad, M. J. A., Santos, A. & Prada, P. O. Linking Gut Microbiota and Inflammation to Obesity and Insulin Resistance. *Physiology (Bethesda)* **31**, 283–293 (2016).

15. Cani, P. D. *et al.* Metabolic endotoxemia initiates obesity and insulin resistance. *Diabetes* **56**, 1761–1772 (2007).

16. Suárez-Zamorano, N. *et al.* Microbiota depletion promotes browning of white adipose tissue and reduces obesity. *Nat. Med.* **21**, 1497–1501 (2015).

17. Virtue, A. T. *et al.* The gut microbiota regulates white adipose tissue inflammation and obesity via a family of microRNAs. *Sci Transl Med* **11**, eaav1892 (2019).

18. Furusawa, Y. *et al.* Commensal microbe-derived butyrate induces the differentiation of colonic regulatory T cells. *Nature* **504**, 446–450 (2013).

19. Inan, M. S. *et al.* The luminal short-chain fatty acid butyrate modulates NF-kappaB activity in a human colonic epithelial cell line. *Gastroenterology* **118**, 724–734 (2000).

20. Besten, G. den *et al.* Short-Chain Fatty Acids Protect Against High-Fat Diet–Induced Obesity via a PPARγ-Dependent Switch From Lipogenesis to Fat Oxidation. *Diabetes* **64**, 2398–2408 (2015).

21. He, Y. *et al.* Regional variation limits applications of healthy gut microbiome reference ranges and disease models. *Nat. Med.* **24**, 1532–1535 (2018).

22. Nishijima, S. *et al.* The gut microbiome of healthy Japanese and its microbial and functional uniqueness. *DNA Res.* **23**, 125–133 (2016).

23. David, L. A. *et al.* Diet rapidly and reproducibly alters the human gut microbiome. *Nature* **505**, 559–563 (2014).

24. Wu, G. D. *et al.* Linking long-term dietary patterns with gut microbial enterotypes. *Science* **334**, 105–108 (2011).

25. De Filippo, C. *et al.* Impact of diet in shaping gut microbiota revealed by a comparative study in children from Europe and rural Africa. *Proc. Natl. Acad. Sci. U.S.A.* **107**, 14691–14696 (2010).

26. Goodrich, J. K. *et al.* Genetic Determinants of the Gut Microbiome in UK Twins. *Cell Host Microbe* **19**, 731–743 (2016).

27. Kasai, C. *et al.* Comparison of the gut microbiota composition between obese and non-obese individuals in a Japanese population, as analyzed by terminal restriction fragment length polymorphism and next-generation sequencing. *BMC Gastroenterol* **15**, 100 (2015).

28. Sato, J. *et al.* Gut dysbiosis and detection of 'live gut bacteria' in blood of Japanese patients with type 2 diabetes. *Diabetes Care* **37**, 2343–2350 (2014).

29. Adachi, K. *et al.* Gut microbiota disorders cause type 2 diabetes mellitus and homeostatic disturbances in gut-related metabolism in Japanese subjects. *J Clin Biochem Nutr* **64**, 231–238 (2019).

30. Tsugane, S. Why has Japan become the world's most long-lived country: insights from a food and nutrition perspective. *Eur J Clin Nutr* **75**, 921–928 (2021).

31. Takada, T., Watanabe, K., Makino, H. & Kushiro, A. Reclassification of Eubacterium desmolans as Butyricicoccus desmolans comb. nov., and description of Butyricicoccus faecihominis sp. nov., a butyrate-producing bacterium from human faeces. *International Journal of Systematic and Evolutionary Microbiology,* **66**, 4125–4131 (2016).

32. Ozato, N. *et al.* Blautia genus associated with visceral fat accumulation in adults 20–76 years of age. *npj Biofilms and Microbiomes* **5**, 1–9 (2019).

33. Tong, X. *et al.* Structural Alteration of Gut Microbiota during the Amelioration of Human Type 2 Diabetes with Hyperlipidemia by Metformin and a Traditional Chinese Herbal Formula: a Multicenter, Randomized, Open Label Clinical Trial. *mBio* **9**, e02392-17 (2018).

34. Patti, M.-E. & Corvera, S. The role of mitochondria in the pathogenesis of type 2 diabetes. *Endocr Rev* **31**, 364–395 (2010).

35. Viola, A., Munari, F., Sánchez-Rodríguez, R., Scolaro, T. & Castegna, A. The Metabolic Signature of Macrophage Responses. *Front Immunol* **10**, 1462 (2019).

36. Wu, Z. *et al.* Mechanisms controlling mitochondrial biogenesis and respiration through the thermogenic coactivator PGC-1. *Cell* **98**, 115–124 (1999).

37. Patel, D. P. *et al.* Metabolic profiling by gas chromatography-mass spectrometry of energy metabolism in high-fat diet-fed obese mice. *PLOS ONE* **12**, e0177953 (2017).

38. Bene, J., Hadzsiev, K. & Melegh, B. Role of carnitine and its derivatives in the development and management of type 2 diabetes. *Nutrition & Diabetes* **8**, 1–10 (2018).

39. Pettegrew, J. W., Levine, J. & McClure, R. J. Acetyl- L -carnitine physical-chemical, metabolic, and therapeutic properties: relevance for its mode of action in Alzheimer's disease and geriatric depression. *Molecular Psychiatry* **5**, 616–632 (2000).

40. Darzi, Y., Letunic, I., Bork, P. & Yamada, T. iPath3.0: interactive pathways explorer v3. *Nucleic Acids Res* **46**, W510–W513 (2018).

41. Kanehisa, M., Furumichi, M., Tanabe, M., Sato, Y. & Morishima, K. KEGG: new perspectives on genomes, pathways, diseases and drugs. *Nucleic Acids Res* **45**, D353–D361 (2017).

42. Park, J. *et al.* Comprehensive analysis of gut microbiota of a healthy population and covariates affecting microbial variation in two large Japanese cohorts. *BMC Microbiol* **21**, 151 (2021).

43. Rontein, D. *et al.* Plants Synthesize Ethanolamine by Direct Decarboxylation of Serine Using a Pyridoxal Phosphate Enzyme*. *Journal of Biological Chemistry* **276**, 35523–35529 (2001).

44. Keshet, R., Szlosarek, P., Carracedo, A. & Erez, A. Rewiring urea cycle metabolism in cancer to support anabolism. *Nat Rev Cancer* **18**, 634–645 (2018).

45. Auner, G. W. *et al.* Applications of Raman spectroscopy in cancer diagnosis. *Cancer Metastasis Rev* **37**, 691–717 (2018).

46. Samuel, A. Z. *et al.* Molecular profiling of lipid droplets inside HuH7 cells with Raman micro-spectroscopy. *Commun Biol* **3**, 372 (2020).

47. Wiercigroch, E. *et al.* Raman and infrared spectroscopy of carbohydrates: A review. *Spectrochim Acta A Mol Biomol Spectrosc* **185**, 317–335 (2017).

48. Blanco, G., Sánchez, B., Fdez-Riverola, F., Margolles, A. & Lourenço, A. In silico Approach for Unveiling the Glycoside Hydrolase Activities in Faecalibacterium prausnitzii Through a Systematic and Integrative Large-Scale Analysis. *Front Microbiol* **10**, 517 (2019).

49. Flint, H. J., Scott, K. P., Duncan, S. H., Louis, P. & Forano, E. Microbial degradation of complex carbohydrates in the gut. *Gut Microbes* **3**, 289–306 (2012).

50. Rios-Covian, D., Gueimonde, M., Duncan, S. H., Flint, H. J. & de los Reyes-Gavilan, C. G. Enhanced butyrate formation by cross-feeding between Faecalibacterium prausnitzii and Bifidobacterium adolescentis. *FEMS Microbiol Lett* **362**, (2015).

51. Segata, N. *et al.* Metagenomic biomarker discovery and explanation. *Genome Biol* **12**, R60 (2011).

52. Louis, P. & Flint, H. J. Formation of propionate and butyrate by the human colonic microbiota. *Environ Microbiol* **19**, 29–41 (2017).

53. Schären, M. *et al.* Differential effects of monensin and a blend of essential oils on rumen microbiota composition of transition dairy cows. *Journal of Dairy Science* **100**, 2765–2783 (2017).

54. Vital, M., Howe, A. C. & Tiedje, J. M. Revealing the bacterial butyrate synthesis pathways by analyzing (meta)genomic data. *mBio* **5**, e00889 (2014).

55. Depommier, C. *et al.* Supplementation with Akkermansia muciniphila in overweight and obese human volunteers: a proof-of-concept exploratory study. *Nat. Med.* **25**, 1096–1103 (2019).

56. Furlow, B. Gut microbe composition and metabolic syndrome. *Lancet Diabetes Endocrinol* **1 Suppl 1**, s4-5 (2013).

57. Salles, B. I. M., Cioffi, D. & Ferreira, S. R. G. Probiotics supplementation and insulin resistance: a systematic review. *Diabetol Metab Syndr* **12**, 98 (2020).

58. Gaike, A. H. *et al.* The Gut Microbial Diversity of Newly Diagnosed Diabetics but Not of Prediabetics Is Significantly Different from That of Healthy Nondiabetics. *mSystems* **5**, e00578-19 (2020).

59. Yan, X., Feng, B., Li, P., Tang, Z. & Wang, L. Microflora Disturbance during Progression of Glucose Intolerance and Effect of Sitagliptin: An Animal Study. *J Diabetes Res* **2016**, 2093171 (2016).

60. Kashtanova, D. A. *et al.* Gut Microbiota in Patients with Different Metabolic Statuses: Moscow Study. *Microorganisms* **6**, E98 (2018).

61. Benítez-Páez, A. *et al.* Depletion of Blautia Species in the Microbiota of Obese Children Relates to Intestinal Inflammation and Metabolic Phenotype Worsening. *mSystems* **5**, e00857-19 (2020).

62. Cancello, R. *et al.* The nicotinic acetylcholine receptor α7 in subcutaneous mature adipocytes: downregulation in human obesity and modulation by diet-induced weight loss. *International Journal of Obesity (2005)* **36**, 1552–1557 (2012).

63. Bencherif, M., Lippiello, P. M., Lucas, R. & Marrero, M. B. Alpha7 nicotinic receptors as novel therapeutic targets for inflammation-based diseases. *Cellular and molecular life sciences: CMLS* **68**, 931–949 (2011).

64. Wang, H. *et al.* Nicotinic acetylcholine receptor alpha7 subunit is an essential regulator of inflammation. *Nature* **421**, 384–388 (2003).

65. Marrero, M. B. *et al.* An alpha7 nicotinic acetylcholine receptor-selective agonist reduces weight gain and metabolic changes in a mouse model of diabetes. *The Journal of Pharmacology and Experimental Therapeutics* **332**, 173–180 (2010).

66. Caspani, G., Kennedy, S., Foster, J. A. & Swann, J. Gut microbial metabolites in depression: understanding the biochemical mechanisms. *Microb Cell* **6**, 454–481 (2019).

67. Stanaszek, P. M., Snell, J. F. & O'Neill, J. J. Isolation, extraction, and measurement of acetylcholine from Lactobacillus plantarum. *Appl Environ Microbiol* **34**, 237–239 (1977).

68. Sugino, T., Shirai, T., Kajimoto, Y. & Kajimoto, O. L-ornithine supplementation attenuates physical fatigue in healthy volunteers by modulating lipid and amino acid metabolism. *Nutr Res* **28**, 738–743 (2008).

69. Acharya, S. K., Bhatia, V., Sreenivas, V., Khanal, S. & Panda, S. K. Efficacy of L-ornithine L-aspartate in acute liver failure: a double-blind, randomized, placebo-controlled study. *Gastroenterology* **136**, 2159–2168 (2009).

70. Saheki, T. *et al.* Comparison of the Urea Cycle in Conventional and Germ-Free Mice. *The Journal of Biochemistry* **88**, 1563–1566 (1980).

71. Jin, C. J. *et al.* S-adenosyl-L-methionine increases skeletal muscle mitochondrial DNA density and whole body insulin sensitivity in OLETF rats. *J Nutr* **137**, 339–344 (2007).

72. Moon, M. K. *et al.* S-Adenosyl-L-methionine ameliorates TNFalpha-induced insulin resistance in 3T3-L1 adipocytes. *Exp Mol Med* **42**, 345–352 (2010).

73. Hardy, M. L. *et al.* S-adenosyl-L-methionine for treatment of depression, osteoarthritis, and liver disease. *Evid Rep Technol Assess (Summ)* 1–3 (2003).

74. Kanai, M., Mizunuma, M., Fujii, T. & Iefuji, H. A genetic method to enhance the accumulation of S-adenosylmethionine in yeast. *Appl Microbiol Biotechnol* **101**, 1351–1357 (2017).

75. Palau-Rodriguez, M. *et al.* Metabolomic insights into the intricate gut microbial-host interaction in the development of obesity and type 2 diabetes. *Front Microbiol* **6**, 1151 (2015).

76. Zhang, L. S. & Davies, S. S. Microbial metabolism of dietary components to bioactive metabolites: opportunities for new therapeutic interventions. *Genome Med* **8**, 46 (2016).

77. Lunn, J. & Buttriss, J. L. Carbohydrates and dietary fibre. *Nutrition Bulletin* **32**, 21–64 (2007).

78. Duncan, S. H. *et al.* Contribution of acetate to butyrate formation by human faecal bacteria. *Br. J. Nutr.* **91**, 915–923 (2004).

79. Rowland, I. *et al.* Gut microbiota functions: metabolism of nutrients and other food components. *Eur J Nutr* **57**, 1–24 (2018).

80. Fernández-Veledo, S. & Vendrell, J. Gut microbiota-derived succinate: Friend or foe in human metabolic diseases? *Rev Endocr Metab Disord* **20**, 439–447 (2019).

81. Hosomi, K. *et al.* Method for preparing DNA from feces in guanidine thiocyanate solution affects 16S rRNA-based profiling of human microbiota diversity. *Sci Rep* **7**, 4339 (2017).

82. Klindworth, A. *et al.* Evaluation of general 16S ribosomal RNA gene PCR primers for classical and next-generation sequencing-based diversity studies. *Nucleic Acids Res.* **41**, e1 (2013).

83. Caporaso, J. G. *et al.* QIIME allows analysis of high-throughput community sequencing data. *Nat. Methods* **7**, 335–336 (2010).

84. Mohsen, A., Park, J., Chen, Y.-A., Kawashima, H. & Mizuguchi, K. Impact of quality trimming on the efficiency of reads joining and diversity analysis of Illumina paired-end reads in the context of QIIME1 and QIIME2 microbiome analysis frameworks. *BMC Bioinformatics* **20**, 581 (2019).

85. Edgar, R. C. Search and clustering orders of magnitude faster than BLAST. *Bioinformatics* **26**, 2460–2461 (2010).

86. Quast, C. *et al.* The SILVA ribosomal RNA gene database project: improved data processing and web-based tools. *Nucleic Acids Res.* **41**, D590-596 (2013).

87. Matsuzaka, T. *et al.* Crucial role of a long-chain fatty acid elongase, Elovl6, in obesity-induced insulin resistance. *Nat. Med.* **13**, 1193–1202 (2007).

88. Nagatake, T. *et al.* The 17,18-epoxyeicosatetraenoic acid-G protein-coupled receptor 40 axis ameliorates contact hypersensitivity by inhibiting neutrophil mobility in mice and cynomolgus macaques. *J. Allergy Clin. Immunol.* **142**, 470-484.e12 (2018).

89. Sasakawa, Y. *et al.* The Anti-obesity and Anti-inflammatory Effects of "LICONINE^{TM}", an Extract of Glycyrrhiza Uralensis, on Diet-induced Obese Mice and 3T3-L1 Mouse Adipocytes. *Journal of Food and Nutrition Research* **5**, 781–788 (2017).

90. Kobayashi, A. *et al.* Metabolomic LC-MS/MS analyses and meta 16S rRNA gene analyses on cecal feces of Japanese rock ptarmigans reveal fundamental differences between semi-wild and captive raised individuals. *J Vet Med Sci* **82**, 1165–1172 (2020).

91. Kubo, A. *et al.* Semi-quantitative analyses of metabolic systems of human colon cancer metastatic xenografts in livers of superimmunodeficient NOG mice. *Anal Bioanal Chem* **400**, 1895–1904 (2011).

92. Horii, S. *et al.* Detection of Penicillin G Produced by Penicillium chrysogenum with Raman Microspectroscopy and Multivariate Curve Resolution-Alternating Least-Squares Methods. *J Nat Prod* **83**, 3223–3229 (2020).

93. Ando, M. & Hamaguchi, H. Molecular component distribution imaging of living cells by multivariate curve resolution analysis of space-resolved Raman spectra. *J Biomed Opt* **19**, 011016

(2014).

94. McMurdie, P. J. & Holmes, S. phyloseq: an R package for reproducible interactive analysis and graphics of microbiome census data. *PLoS One* **8**, e61217 (2013).

95. Oksanen, J. *et al.* The vegan Package. *Community ecology package* **10**, 631–637 (2008).

96. Dray, S. & Dufour, A.-B. The ade4 Package: Implementing the Duality Diagram for Ecologists. *Journal of Statistical Software* **22**, 1–20 (2007).

97. Wickham, H. ggplot2: Elegant Graphics for Data Analysis. Springer-Verlag New York. ISBN 978-3-319-24277-4. *Springer-Verlag New York* https://cran.r-project.org/web/packages/ggplot2/citation.html (2016).

98. Barter, R. L. & Yu, B. Superheat: An R package for creating beautiful and extendable heatmaps for visualizing complex data. *J Comput Graph Stat* **27**, 910–922 (2018).

Figures

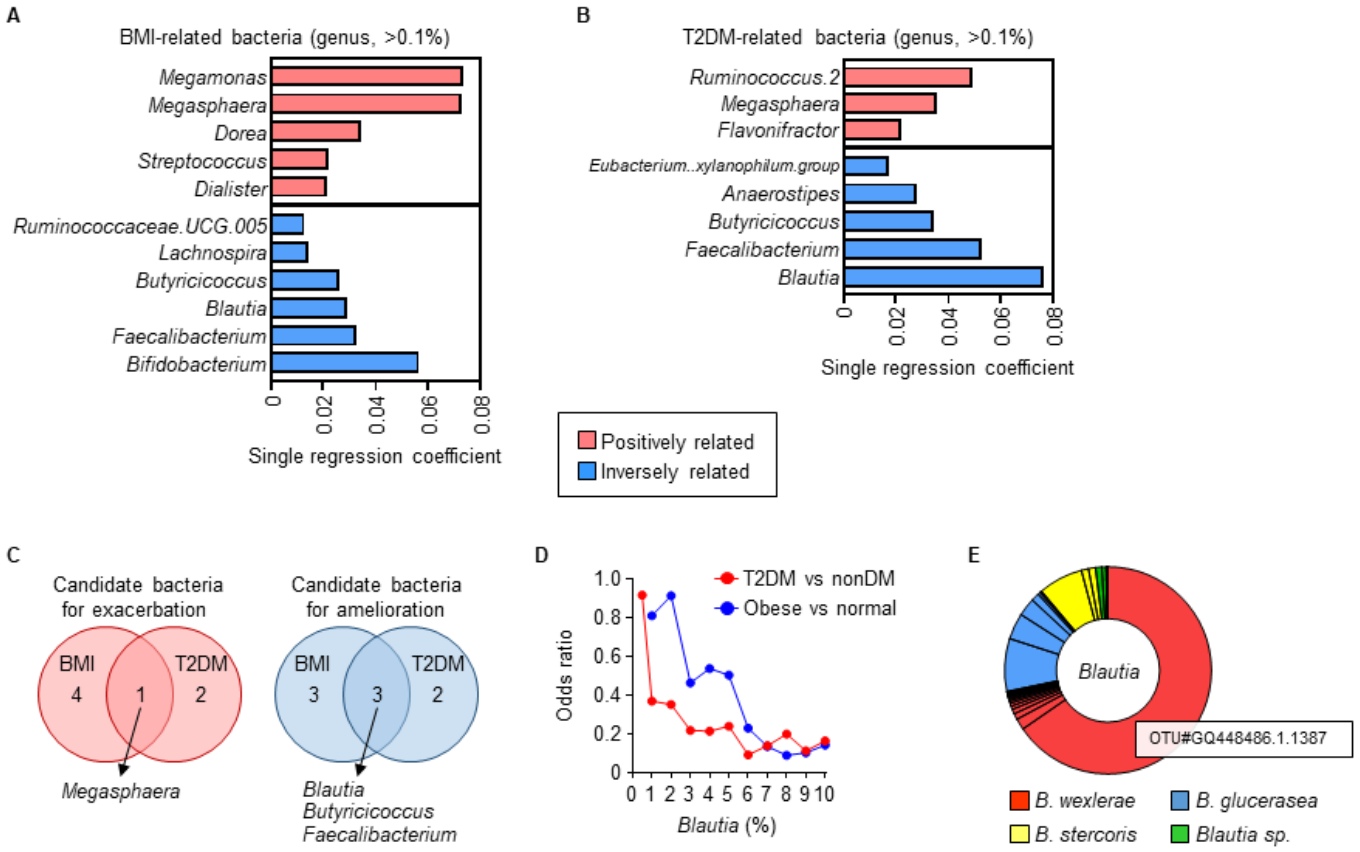

Figure 1

Figure 1

Intestinal bacterial genera associated with body mass index (BMI) and type 2 diabetes mellitus (T2DM) in Japanese adults.

(A) BMI-related bacterial genera, which are selected and ranked according to R^2 score from single regression analysis ($P < 0.05$) among 16 genera that were identified by multiple regression analysis by forward selection (Table S2). (B) T2DM-related bacterial genera, which are selected and ranked according to R^2 score from single regression analysis ($P < 0.05$) among 22 genera that were identified by multiple logistic regression analysis by forward selection (Table S3). (C) Intestinal genera associated with both BMI and T2DM. (D) Odds ratios for *Blautia* abundance in the development of obesity (BMI ≥ 25) and T2DM. (E) Estimation of *Blautia* species according to BlastN analysis of representative OTU sequences.

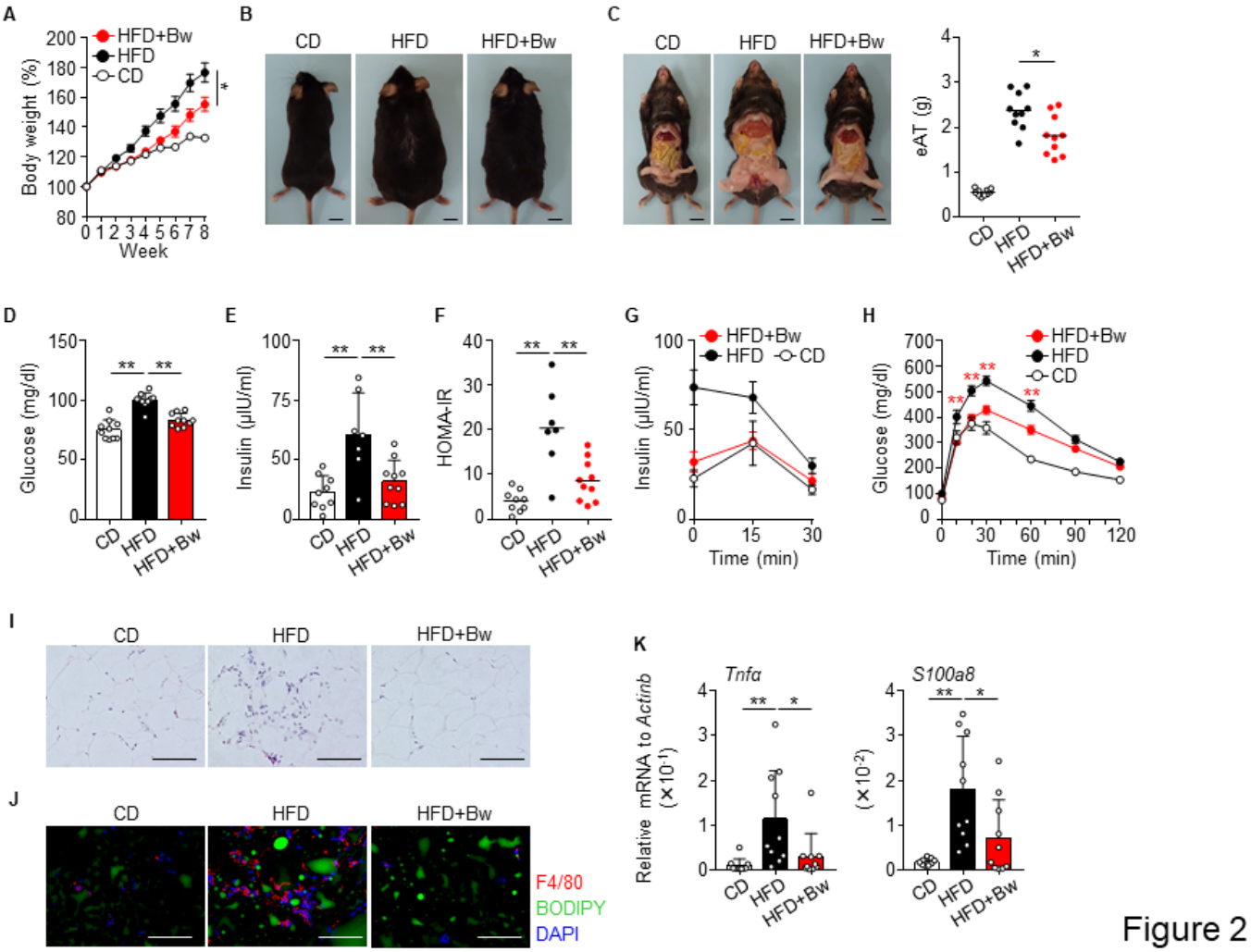

Figure 2

Figure 2

High-fat diet (HFD)-induced obesity and diabetes were ameliorated by oral administration of *Blautia wexlerae* to mice.

(A) Mice were maintained for 8 weeks on standard chow (control diet, CD) or HFD without or with oral administration of *B. wexlerae* (Bw) 3 times each week and were weighed weekly (n = 5, mean ± 1 SD). (B) Photographs of representative mice. (C) Photographs of representative mice and weight of epididymal adipose tissue (eAT). (D) Fasting blood glucose. (E) Fasting blood insulin. (F) HOMA-IR, an indicator of insulin resistance, calculated as 'glucose (mg/dl) × insulin (μU/ml) / 405'. (G) Blood insulin was monitored through intraperitoneal glucose tolerance testing (IPGTT; n = 10, mean ± 1 SD). (H) Blood glucose was monitored by using IPGTT (n = 10, mean ± SD). (I) Hematoxylin–eosin staining of eAT. Scale bar, 100 μm. (J) Immunohistologic analysis of eAT. Macrophages, lipid droplets, and nuclei were visualized by using F4/80 monoclonal antibody (red), BODIPY (green), and DAPI (blue) staining, respectively. Scale bar, 100 μm. (K) Gene expression of *Tnfa*, an inflammatory cytokine, and *S100a8*, a chemokine for recruiting macrophages, in the eAT mature adipocyte fraction (MAF). Statistical

significance was evaluated by using one-way ANOVA; *$P < 0.05$, **$P < 0.01$. CD, lean mice fed a standard chow diet (CD-fed mice); HFD, obese mice fed a high-fat diet (HFD-fed mice); HFD+Bw, HFD-fed mice orally supplemented with *B. wexlerae*.

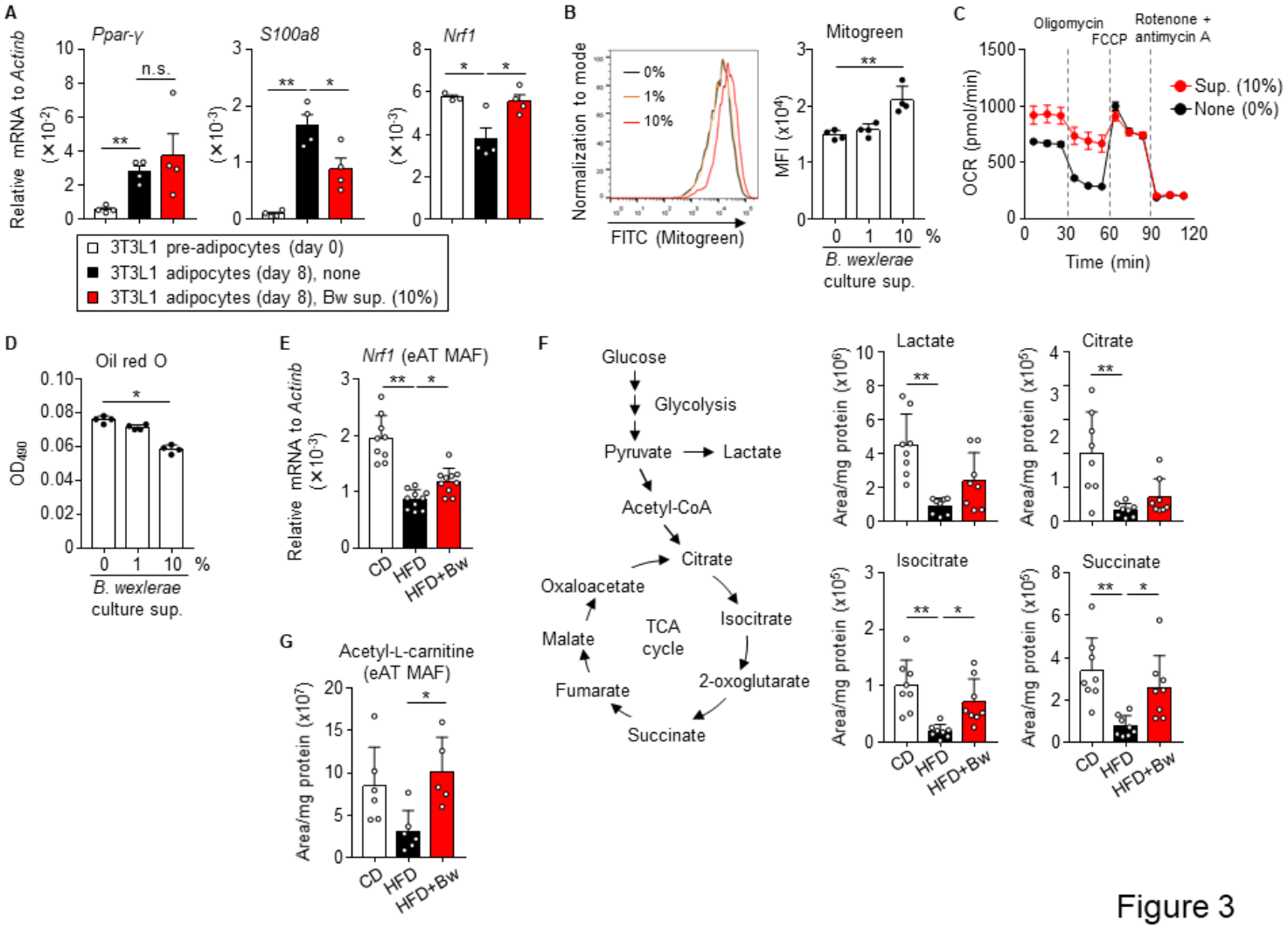

Figure 3

Figure 3

Blautia wexlerae-derived metabolites showed anti-inflammatory and anti-adipogenesis properties in adipocytes as well as alteration of mitochondrial metabolism.

(A) 3T3L1 pre-adipocytes were differentiated into mature adipocytes in the absence (none) or presence of the cultured supernatant of *B. wexlerae* at a final concentration of 10%. Gene expression of *Pparγ* (a transcription factor used as a marker of adipocyte differentiation), *S100a8* (a chemokine for recruiting macrophages), and *Nrf1* (a transcriptional factor used as a marker of mitochondrial biogenesis) was measured in 3T3L1 pre-adipocytes and adipocytes. (B) Mitochondrial mass was measured by flow cytometry analysis using Mitogreen in 3T3L1 adipocytes treated without or with culture supernatant (sup.) of *B. wexlerae* at a final concentration of 1% or 10%. (C) By using an XF24 extracellular flux analyzer, the oxygen consumption rate (OCR) was measured in 3T3L1 adipocytes treated without or with

the cultured supernatant of *B. wexlerae* at the concentration of 10%. (D) Lipid accumulation was assessed by using oil red O staining in 3T3L1 adipocytes treated without or with culture supernatant of *B. wexlerae* at a final concentration of 1% or 10%. (E) Gene expression of *Nrf1* in the eAT MAF of mice. (F) Representative metabolites of glycolysis (lactate) and the TCA cycle (citrate, isocitrate, and succinate) in the eAT MAF of mice were measured by using liquid chromatography-tandem mass spectroscopy (LC-MS/MS). (G) Acetyl-l-carnitine, a constituent of the inner mitochondrial membrane, in the eAT MAF of mice was measured by using LC-MS/MS. Statistical significance was evaluated by using one-way ANOVA; n.s., not significant; $*P < 0.05$; $**P < 0.01$. CD, CD-fed mice; HFD, HFD-fed mice, HFD+Bw, HFD-fed mice supplemented with *B. wexlerae*.

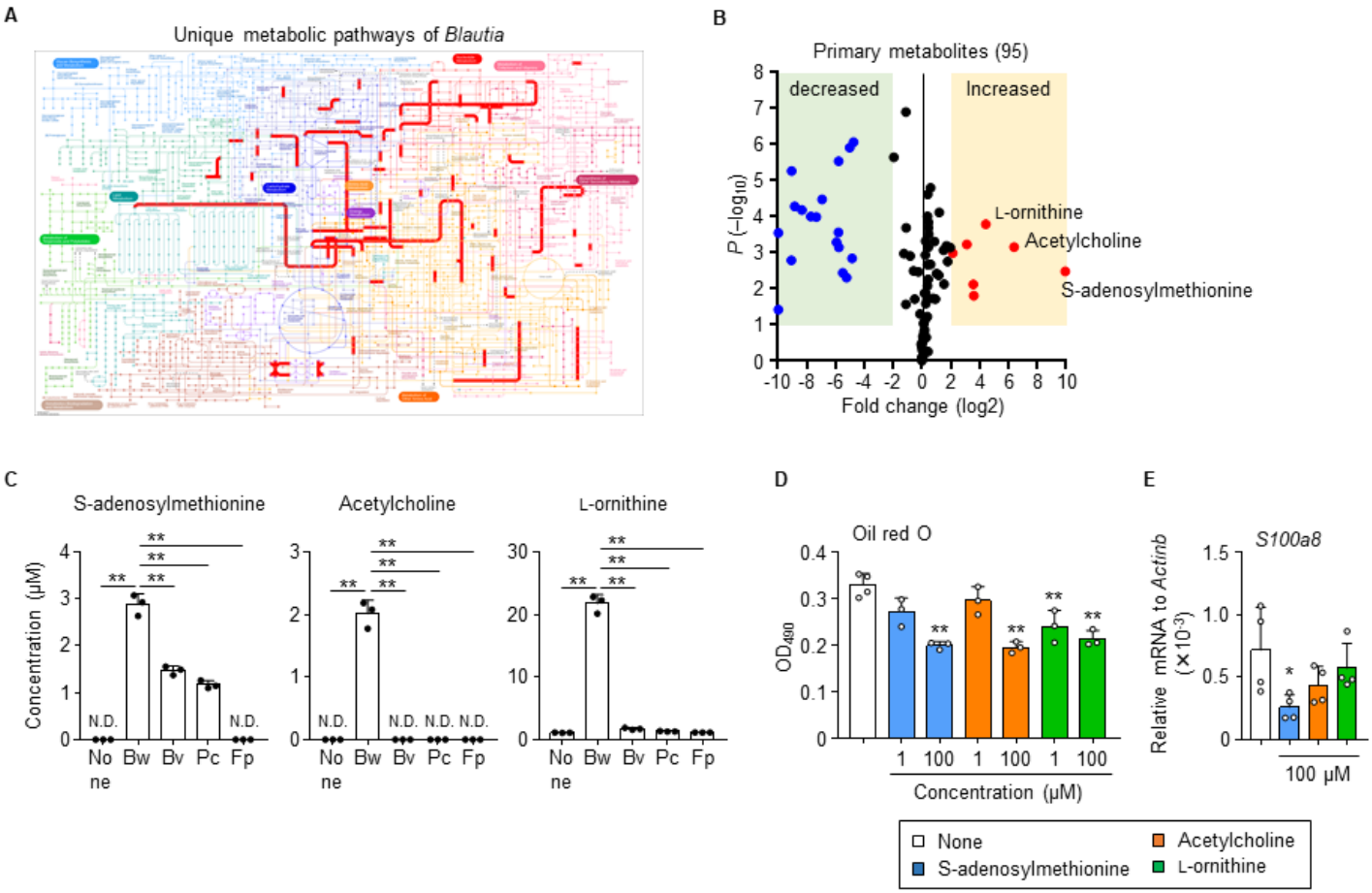

Figure 4

Figure 4

Blautia wexlerae showed unique characteristics in amino acid metabolism, such as production of S-adenosylmethionine, acetylcholine, and l-ornithine.

(A) Unique metabolic pathways (red lines) of *Blautia* (KEGG organism code: rob) in comparison with major intestinal bacteria, including *Bacteroides* (KEGG organism code: bvu), *Prevotella* (KEGG organism

code: pru), and *Faecalibacterium* (KEGG organism code: fpr), according to the presence of KEGG orthologous groups by using iPATH3.0. (B) Volcano plot showing LC-MS/MS analysis of *B. wexlerae* culture supernatant. Red and blue dots indicate metabolites increased and decreased, respectively, by more than 4-fold in *B. wexlerae* culture supernatant compared with fresh medium (n = 4). (C) Quantitative measurement by LC-MS/MS of S-adenosylmethionine, acetylcholine, and l-ornithine in fresh medium (none) and culture supernatants of *B. wexlerae* (Bw) and major intestinal bacteria including *Bacteroides vulgatus* (Bv), *Prevotella copri* (Pc), and *Faecalibacterium prausnitzii* (Fp). N.D., not detected. (D) Lipid accumulation was measured by oil red O staining in 3T3L1 adipocytes treated without (none) or with S-adenosylmethionine, acetylcholine, and l-ornithine at the concentration of 1 or 100 μM. (E) Gene expression of *S100a8*, a chemokine for recruiting macrophages, in 3T3L1 adipocytes treated without (none) or with S-adenosylmethionine, acetylcholine, and l-ornithine at 100 μM. Statistical significance was evaluated by using one-way ANOVA; **P* < 0.05; ***P* < 0.01.

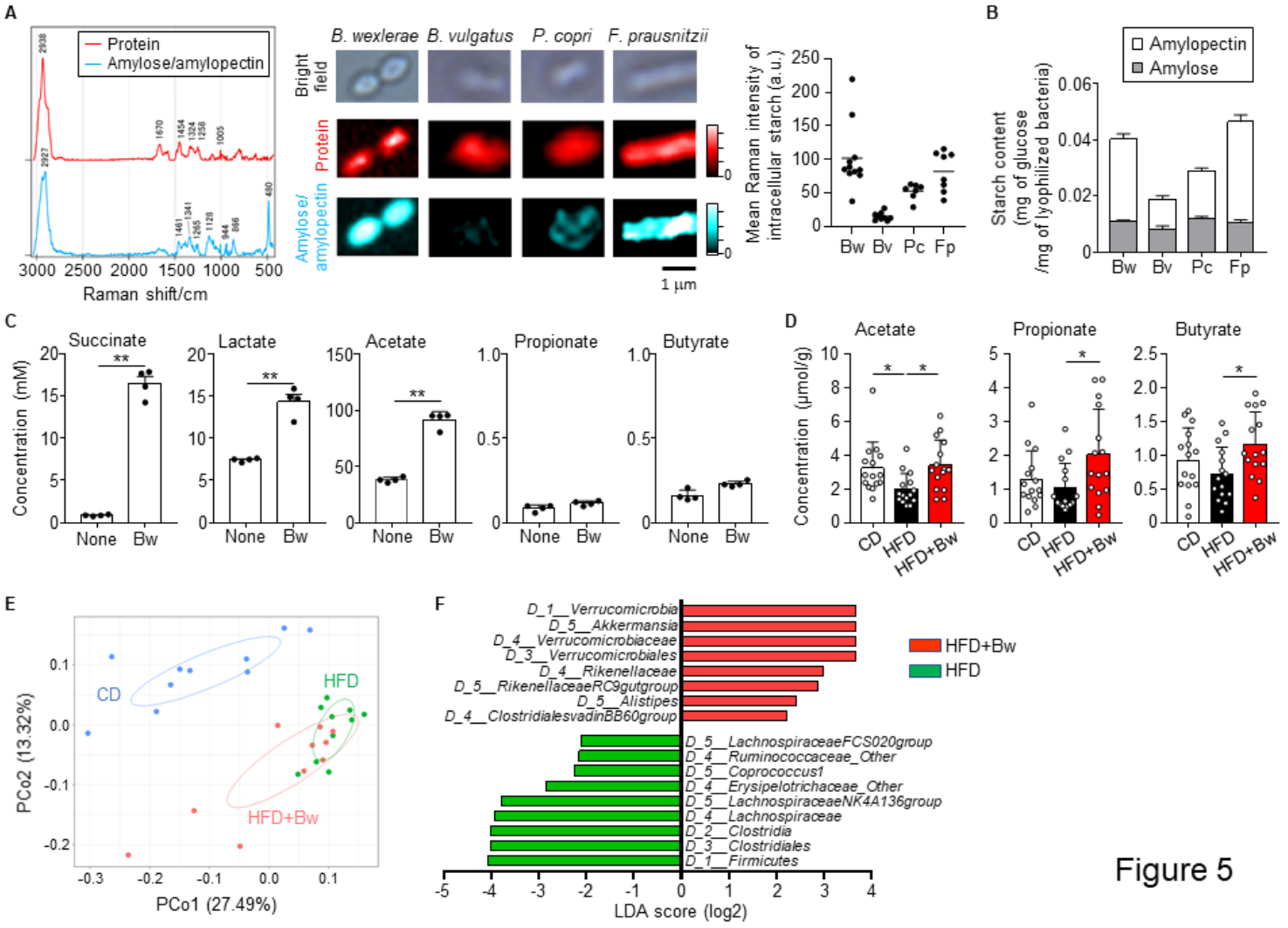

Figure 5

Figure 5

Administration of *B. wexlerae* altered the intestinal environment, including gut bacterial composition and fecal short-chain fatty acid (SCFA) content, in mice.

(A) Raman spectroscopic analysis. Raman shift signals specific for protein and starch were plotted on bacterial cells of *B. wexlerae* (Bw) and major intestinal bacteria including *Bacteroide vulgatus* (Bv), *Prevotella copri* (Pc), and *Faecalibacterium prausnitzii* (Fp). (B) Starch (amylose and amylopectin) contents in *B. wexlerae* (Bw) and major intestinal bacteria, including *B. vulgatus* (Bv), *P. copri* (Pc), and *F. prausnitzii* (Fp). (C) The concentrations of succinate, lactate, acetate, propionate, propionate, and butyrate in fresh medium (none) and *B. wexlerae* culture supernatant (Bw). (D) SCFA content in fecal samples from mice. Mice were maintained on CD or HFD for 8 weeks with or without oral administration of *B. wexlerae* 3 times each week, after which fecal SCFAs were measured by HPLC (E) Principal coordinate analysis (PCoA) of fecal bacterial composition in mice according to the Bray–Curtis distance at genus level. Mice were maintained on CD or HFD for 8 weeks with or without oral administration of *B. wexlerae* 3 times each week, after which fecal bacterial composition was analyzed by 16S amplicon sequencing. (F) Differences in bacterial taxonomy were ranked according to the linear discriminant analysis (LDA) effect size between HFD-fed mice and HFD-fed mice supplemented with *B. wexlerae*. Statistical significance was evaluated by using one-way ANOVA; n.s., not significant; **P* < 0.05; ***P* < 0.01. CD, CD-fed mice; HFD, HFD-fed mice, HFD+Bw, HFD-fed mice supplemented with *B. wexlerae*.

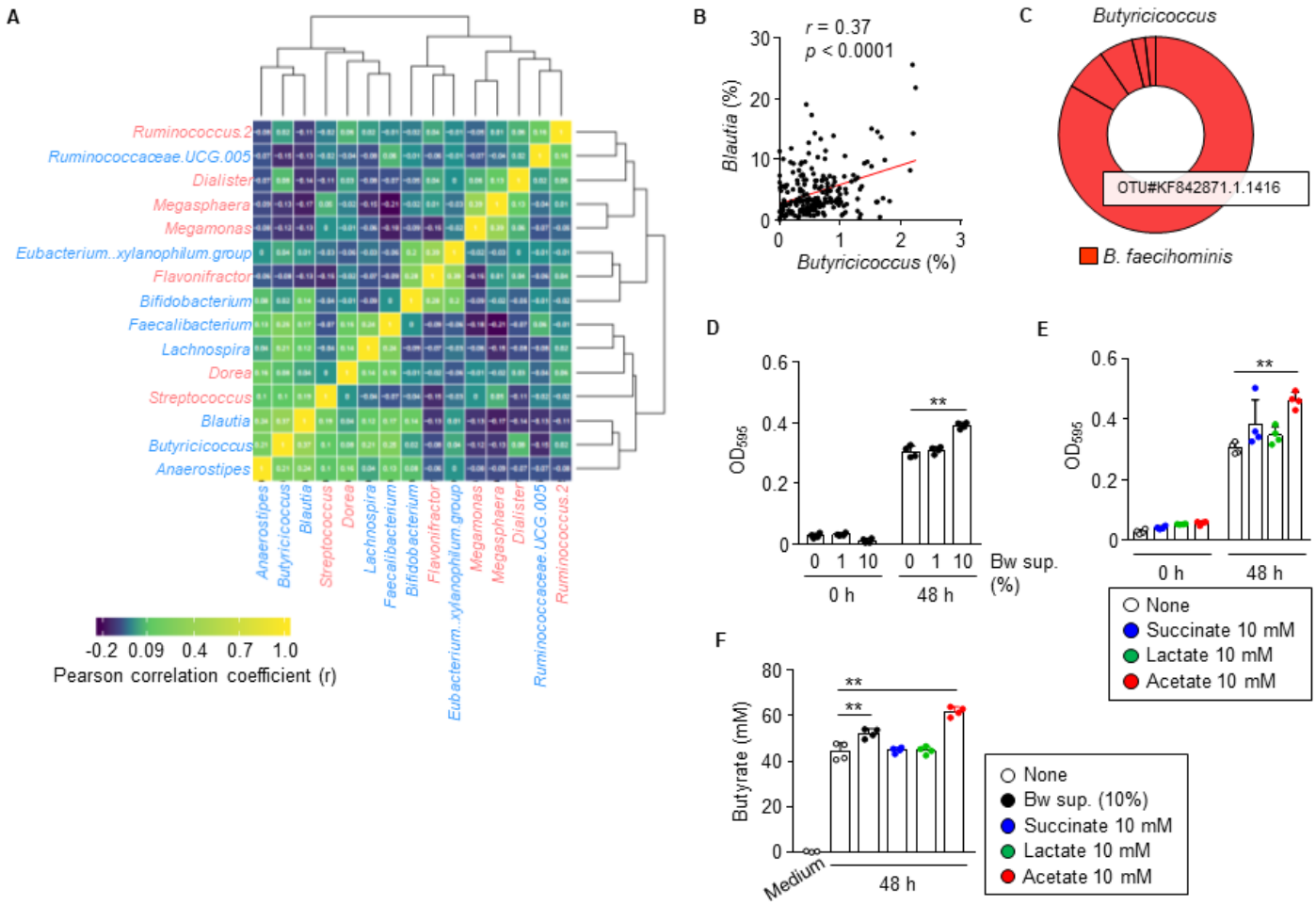

Figure 6

Figure 6

Interaction between *B. wexlerae* and butyrate-producing bacteria.

(A) Heatmap showing correlated relationship among human intestinal bacteria (n = 217). Red and blue fonts indicate bacterial genera from Figure 1 that were positively or inversely, respectively, related to BMI/T2DM. (B) Positive correlation between *Blautia* and *Butyricicoccus* in human fecal samples (n = 217). (C) Estimation of *Butyricicoccus* species according to BlastN analysis of representative OTU sequences. (D) The absorbance of *Butyricicoccus faecihominis*-cultured medium in which the organisms were grown in the absence or presence of *B. wexlerae*-cultured medium at a final concentration of 1% or 10%. (E) The absorbance of *B. faecihominis*-cultured medium in which the organisms were grown in the absence (none) or presence of 10 mM succinate, 10 mM lactate, or 10 mM acetate. (F) The concentration of butyrate in *B. faecihominis*-cultured medium in which the organisms were grown in the absence (none) or presence of *B. wexlerae* culture supernatant at 10%, 10 mM succinate, 10 mM lactate, or 10 mM acetate. Statistical significance was evaluated by using one-way ANOVA; ** $P < 0.01$ (D–F).

Supplementary Files

This is a list of supplementary files associated with this preprint. Click to download.

- 7.tif
- 8.tif
- 9.tif
- 11.tif
- 12.tif
- 13.tif
- 14.tif
- 15.tif
- 16.tif
- 17.tif
- 18.tif
- 19.tif
- 20.tif
- 21.tif
- 22.tif
- 23.tif
- 24.tif